

Robust Tensor Completion Using Transformed Tensor SVD

Guangjing Song*, Michael K. Ng[†] and Xiongjun Zhang[‡]

July 3, 2019

Abstract

In this paper, we study robust tensor completion by using transformed tensor singular value decomposition (SVD), which employs unitary transform matrices instead of discrete Fourier transform matrix that is used in the traditional tensor SVD. The main motivation is that a lower tubal rank tensor can be obtained by using other unitary transform matrices than that by using discrete Fourier transform matrix. This would be more effective for robust tensor completion. Experimental results for hyperspectral, video and face datasets have shown that the recovery performance for the robust tensor completion problem by using transformed tensor SVD is better in PSNR than that by using Fourier transform and other robust tensor completion methods.

Key Words: Robust tensor completion, transformed tensor singular value decomposition, unitary transform matrix, low-rank, sparsity

Mathematics Subject Classification 2010: 15A04, 65F99, 90C25

1 Introduction

Tensor (multi-dimensional arrays) are generalizations of vectors and matrices, which can be used as a powerful tool in modeling multi-dimensional data such as videos [29], color images [36, 40], hyperspectral images [11, 35, 49], and electroencephalography (EEG) [8]. Based on its multilinear algebraic properties, a tensor can take full advantage of its structures to provide better understanding and higher accuracy of the multi-dimensional data. In many tensor data applications [9, 20, 27, 33, 37, 40, 41, 47, 50], tensor data sets are often corrupted and/or incomplete owing to various unpredictable or unavoidable situations. It is motivated us to perform tensor completion and tensor robust principal component analysis for multi-dimensional data processing.

Compared with matrix completion and robust principal component analysis, tensor completion and tensor robust principal component analysis are far from being well-studied. The main issues are the definitions of tensor ranks and tensor decompositions. In the matrix case, it has been shown that the

*School of Mathematics and Information Sciences, Weifang University, Weifang 261061, P.R. China (e-mail: sgjshu@163.com).

[†]Centre for Mathematical Imaging and Vision and Department of Mathematics, Hong Kong Baptist University, Kowloon Tong, Hong Kong (e-mail: mng@math.hkbu.edu.hk). Research supported in part by the HKRGC GRF 12306616, 12200317 and 12300218.

[‡]School of Mathematics and Statistics and Hubei Key Laboratory of Mathematical Sciences, Central China Normal University, Wuhan 430079, China (e-mail: xjzhang@mail.ccnu.edu.cn). Research supported in part by the National Natural Science Foundation of China under grants 11801206, 11571098, 11871025, Hubei Provincial Natural Science Foundation of China under grant 2018CFB105, and Fundamental Research Funds for the Central Universities under grant CCNU19ZN017.

nuclear norm is the convex envelope of the matrix rank over a unit ball of spectral norm [12, 43]. By solving a convex programming problem, one can recover a low rank matrix exactly with overwhelming probability, from a small fraction of its entries, even part of them are corrupted, provided that the corruptions are reasonably sparse [4, 5, 7, 39, 42].

Unlike the matrix case, there exist different kinds of definitions of ranks of a tensor. For instance, the CANDECOMP/PARAFAC (CP) rank is defined as the minimal number of the rank one outer products of tensors, which is NP-hard to compute in general [26]. Although many authors [19, 22] have recovered some special low CP rank tensors by different methods, it is often computationally intractable to determine the CP rank or its best convex approximation. Tensor Train (TT) rank [38] is generated by the TT decomposition using the link structure of each core tensor. Since the link structure, the TT rank is only efficient for higher order tensor for tensor completion. Bengua et al. [2] proposed a novel approach based on TT rank for color images and videos completion. However, this method may be challenged when the third-dimension of the data is high, such as hyperspectral data. The Tucker rank (multi-rank) is actually a vector whose entries can be derived from the factors of Tucker decomposition [45]. Liu et al. [29] proposed to use the sum of the nuclear norms of unfolding matrices of a tensor to recover a low Tucker rank tensor. However, the sum of the nuclear norms of unfolding matrices of a tensor is not the convex envelope of the sum of ranks of unfolding matrices of a tensor [44]. Moreover, Mu et al. [34] showed that the sum of nuclear norms of unfolding matrices of a tensor is suboptimal and proposed a square deal method to recover a low rank and high-order tensor. While the square deal method only utilizes one mode information of unfolding matrices for third-order tensors. Other extensions can be found in [13] and references therein. In [16], Gu et al. provided a perfect recovery of two components (the low-rank tensor and the entrywise sparse corruption tensor) under restricted eigenvalue conditions. In [18], Huang et al. proposed a tensor robust principal component analysis model for exact recovery guarantee under certain tensor incoherence conditions.

The tensor-tensor product (t-product) and associated algebraic construction based on the Fourier transform, cosine transform and any invertible transform for tensors of order three or higher are studied in [23, 25, 32], respectively. With this framework, Kilmer et al. [25] introduced an SVD-like factorization called the tensor SVD as well as the definition of tubal rank. Compared with other tensor decompositions, this tensor SVD has been shown to be superior in capturing the spatial-shifting correlation that is ubiquitous in real-world data [24, 25, 32, 51, 53]. Moreover, the tubal nuclear norm is the convex envelope of the tubal average rank within the unit ball of the tensor spectral norm. Motivated by the above results, Zhang et al. [52] derived theoretical performance bounds of the model proposed in [53] using the tensor SVD algebraic framework for third-order tensor recovery from limited sampling. Zhou et al. [54] proposed a novel factorization method based on the tensor nuclear norm in the Fourier domain for solving the third-order tensor completion problem. Hu et al. [17] proposed a twist tensor nuclear norm for tensor completion, which relaxes the tensor multi-rank of the twist tensor in the Fourier domain. Being different from tensor completion, robust tensor completion is more complex due to the sparse noise in the observations. Jiang and Ng [21] showed that one can recover a low tubal rank tensor exactly with overwhelming probability by simply solving a convex program, where the objective function is a weighted combination of tubal nuclear norm, a convex surrogate of the tubal-rank, and the ℓ_1 -norm. Recently, Lu et al. [31] considered the tensor robust principal component analysis problem and proposed a tensor nuclear norm based on t-product and tensor SVD in the Fourier domain, where the theoretical guarantee for the exact recovery was also provided.

The main aim of this paper is to study robust tensor completion problems by using transformed tensor SVD, which employs unitary transform matrices instead of discrete Fourier transform matrix in the tensor SVD. The main motivation is that a lower tubal rank tensor can be obtained by using other unitary transform matrices than that by using discrete Fourier transform matrix. This would be more effective for robust tensor completion. The main contributions of this paper are given as follows. (i)

One can recover a low transformed tubal rank tensor exactly with overwhelming probability provided that its rank is sufficiently small and its corrupted entries are reasonably sparse. Because of the use of unitary transformation, there are new results in the convex envelope of rank, the subgradient formula and tensor basis required in the proof. (ii) We propose a new unitary transformation that can lead to significant recovery results compared with the use of the Fourier transform. (iii) Experimental results for hyperspectral and face images and video data have shown that the recovery performance by using transformed tensor SVD is better in PSNR than that by using Fourier transform in tensor SVD and other tensor completion methods.

The outline of this paper is given as follows. In Section 2, we introduce transformed tensor SVD. In Section 3, we analyze the robust tensor completion problem and the algorithm for solving the model. In Section 4, numerical results are presented to show that the effectiveness of the proposed tensor SVD for the robust tensor completion problem. Finally, some concluding remarks are given in Section 5. All proofs are deferred to the Appendix.

1.1 Notation and Preliminaries

Throughout this paper, the fields of real number and complex number are denoted as \mathbb{R} and \mathbb{C} , respectively. Tensors and matrices are denoted by Euler letters and boldface capital letters, respectively. For a third-order tensor $\mathcal{A} \in \mathbb{R}^{n_1 \times n_2 \times n_3}$, we denote its (i, j, k) -th entry as \mathcal{A}_{ijk} and use the Matlab notation $\mathcal{A}(i, :, :)$, $\mathcal{A}(:, i, :)$ and $\mathcal{A}(:, :, i)$ to denote the i -th horizontal, lateral and frontal slices, respectively. Specifically, the frontal slice $\mathcal{A}(:, :, i)$ is denoted compactly as $\mathcal{A}^{(i)}$. $\mathcal{A}(i, j, :)$ denotes a tubal fiber obtained by fixing the first two indices and varying the third index. Moreover, a tensor tube of size $1 \times 1 \times n_3$ is denoted as $\hat{\mathbf{a}}$ and a tensor column of size $n_1 \times 1 \times n_3$ is denoted as $\vec{\mathbf{a}}$.

The inner product of $\mathbf{A}, \mathbf{B} \in \mathbb{C}^{n_1 \times n_2}$ is given by $\langle \mathbf{A}, \mathbf{B} \rangle = \text{Tr}(\mathbf{A}^H \mathbf{B})$, where \mathbf{A}^H denotes the conjugate transpose of \mathbf{A} and $\text{Tr}(\cdot)$ denotes the matrix trace. For a vector $v \in \mathbb{C}^n$, the l_2 -norm is $\|v\|_2 = \sqrt{\sum_i |v_i|^2}$. The spectral norm of a matrix $\mathbf{A} \in \mathbb{C}^{n_1 \times n_2}$ is denoted as $\|\mathbf{A}\| = \max_i \sigma_i(\mathbf{A})$, where $\sigma_i(\mathbf{A})$ is the i -th largest singular value of \mathbf{A} . The nuclear norm of a matrix is defined as $\|\mathbf{A}\|_* = \sum_i \sigma_i(\mathbf{A})$. For a tensor \mathcal{A} , the l_1 -norm is defined as $\|\mathcal{A}\|_1 = \sum_{i,j,k} |\mathcal{A}_{ijk}|$, the infinity norm is defined as $\|\mathcal{A}\|_\infty = \max_{i,j,k} |\mathcal{A}_{ijk}|$ and the Frobenius norm is defined as $\|\mathcal{A}\|_F = \sqrt{\sum_{i,j,k} |\mathcal{A}_{ijk}|^2}$. Suppose that \mathbf{L} is a tensor operator, then its operator norm is defined as $\|\mathbf{L}\|_{\text{op}} = \sup_{\|\mathcal{A}\|_F \leq 1} \|\mathbf{L}(\mathcal{A})\|_F$.

2 Transformed Tensor Singular Value Decomposition

Let Φ be the unitary transform matrix with $\Phi\Phi^H = \Phi^H\Phi = \mathbf{I}$, where \mathbf{I} is the identity matrix. $\hat{\mathcal{A}}_\Phi$ represents a third-order tensor obtained via multiplying by Φ on all tubes along the third dimension of \mathcal{A} , i.e.,

$$\text{vec}(\hat{\mathcal{A}}_\Phi(i, j, :)) = \Phi(\text{vec}(\mathcal{A}(i, j, :))),$$

where $\text{vec}(\cdot)$ is the vectorization operator that maps the tensor tube to a vector. Here we write $\hat{\mathcal{A}}_\Phi = \Phi[\mathcal{A}]$. Moreover, one can get \mathcal{A} from $\hat{\mathcal{A}}_\Phi$ by using Φ^H operation along the third-dimension of $\hat{\mathcal{A}}_\Phi$, i.e., $\mathcal{A} = \Phi^H[\hat{\mathcal{A}}_\Phi]$.

We construct a block diagonal matrix based on the frontal slices of \mathcal{A} as follows:

$$\bar{\mathcal{A}} = \text{blockdiag}(\mathcal{A}) := \begin{pmatrix} \mathcal{A}^{(1)} & & & \\ & \mathcal{A}^{(2)} & & \\ & & \ddots & \\ & & & \mathcal{A}^{(n_3)} \end{pmatrix},$$

Also we can convert the block diagonal matrix into a tensor by the following fold operator:

$$\text{fold}(\text{blockdiag}(\mathcal{A})) = \text{fold}(\overline{\mathcal{A}}) := \mathcal{A}.$$

Kernfeld et al. [23] defined the $\star_{\mathbf{L}}$ -product between two tensors by the slices products in the transform domain, where \mathbf{L} is an arbitrary invertible transform. In this paper, we are mainly interested in the t-product which is based on unitary transforms.

Definition 1 The Φ -product of $\mathcal{A} \in \mathbb{C}^{n_1 \times n_2 \times n_3}$ and $\mathcal{B} \in \mathbb{C}^{n_2 \times n_4 \times n_3}$ is a tensor $\mathcal{C} \in \mathbb{C}^{n_1 \times n_4 \times n_3}$, which is given by

$$\mathcal{C} = \mathcal{A} \diamond_{\Phi} \mathcal{B} = \Phi^H \left[\text{fold} \left(\text{blockdiag}(\hat{\mathcal{A}}_{\Phi}) \times \text{blockdiag}(\hat{\mathcal{B}}_{\Phi}) \right) \right],$$

where “ \times ” denotes the standard matrix product.

The t-product [25] of $\mathcal{A} \in \mathbb{R}^{n_1 \times n_2 \times n_3}$ and $\mathcal{B} \in \mathbb{R}^{n_2 \times n_4 \times n_3}$ is a tensor $\mathcal{C} \in \mathbb{R}^{n_1 \times n_4 \times n_3}$ given by

$$\mathcal{C} = \mathcal{A} * \mathcal{B} = \text{Fold}_{vec}(\text{Circ}(\mathcal{A}) \times \text{Vec}(\mathcal{B})), \quad (2.1)$$

where Fold_{vec} is an operation that takes $\text{Vec}(\mathcal{B})$ into a tensor, i.e., $\text{Fold}_{vec}(\text{Vec}(\mathcal{B})) = \mathcal{B}$,

$$\text{Vec}(\mathcal{B}) = \begin{pmatrix} \mathcal{B}^{(1)} \\ \mathcal{B}^{(2)} \\ \vdots \\ \mathcal{B}^{(n_3)} \end{pmatrix},$$

and

$$\text{Circ}(\mathcal{A}) = \begin{pmatrix} \mathcal{A}^{(1)} & \mathcal{A}^{(n_3)} & \mathcal{A}^{(n_3-1)} & \dots & \mathcal{A}^{(2)} \\ \mathcal{A}^{(2)} & \mathcal{A}^{(1)} & \mathcal{A}^{(n_3)} & \dots & \mathcal{A}^{(3)} \\ \vdots & \ddots & \ddots & \ddots & \vdots \\ \mathcal{A}^{(n_3)} & \mathcal{A}^{(n_3-1)} & \dots & \mathcal{A}^{(2)} & \mathcal{A}^{(1)} \end{pmatrix}.$$

The t-product (2.1) can be seen as a special case of Definition 1. Recall that the block circulant matrix $\text{Circ}(\mathcal{A})$ can be diagonalized by the discrete Fourier transform matrix \mathbf{F}_{n_3} and the diagonal matrices are the frontal slices of $\hat{\mathcal{A}}_{\mathbf{F}_{n_3}}$, i.e.,

$$(\mathbf{F}_{n_3} \otimes I_{n_1}) \times \text{Circ}(\mathcal{A}) \times (\mathbf{F}_{n_3}^H \otimes I_{n_2}) = \text{blockdiag}(\hat{\mathcal{A}}_{\mathbf{F}_{n_3}}),$$

where \otimes is the Kronecker product. It follows that

$$\begin{aligned} \mathcal{A} * \mathcal{B} &= \text{Fold}_{vec}(\text{Circ}(\mathcal{A}) \times \text{Vec}(\mathcal{B})) \\ &= \text{Fold}_{vec} \left((\mathbf{F}_{n_3}^H \otimes I_{n_1}) \times \text{blockdiag}(\hat{\mathcal{A}}_{\mathbf{F}}) \times (\mathbf{F}_{n_3} \otimes I_{n_2}) \times \text{Vec}(\mathcal{B}) \right) \\ &= \text{Fold}_{vec} \left((\mathbf{F}_{n_3}^H \otimes I_{n_1}) \times \text{blockdiag}(\hat{\mathcal{A}}_{\mathbf{F}}) \times \text{Vec}(\hat{\mathcal{B}}_{\mathbf{F}}) \right) \\ &= \text{fold} \left((\mathbf{F}_{n_3}^H \otimes I_{n_1}) \times \text{blockdiag}(\hat{\mathcal{A}}_{\mathbf{F}}) \times \text{blockdiag}(\hat{\mathcal{B}}_{\mathbf{F}}) \right) \\ &= \mathbf{F}_{n_3}^H \left[\text{fold} \left(\text{blockdiag}(\hat{\mathcal{A}}_{\mathbf{F}}) \times \text{blockdiag}(\hat{\mathcal{B}}_{\mathbf{F}}) \right) \right] \\ &= \mathcal{A} \diamond_{\mathbf{F}_{n_3}} \mathcal{B}. \end{aligned}$$

According to Φ -product, we have the definitions of the conjugate transpose of \mathcal{A} , the identity tensor, the unitary tensor, and the inner product between two tensors.

Definition 2 The conjugate transpose of $\mathcal{A} \in \mathbb{C}^{n_1 \times n_2 \times n_3}$ with respect to Φ is the tensor $\mathcal{A}^H \in \mathbb{C}^{n_2 \times n_1 \times n_3}$ obtained by

$$\mathcal{A}^H = \Phi^H \left[\text{fold} \left(\text{blockdiag}(\hat{\mathcal{A}}_\Phi)^H \right) \right].$$

Definition 3 [23, Proposition 4.1] The identity tensor $\mathcal{I}_\Phi \in \mathbb{C}^{n \times n \times n_3}$ (with respect to Φ) is defined to be a tensor such that $\mathcal{I}_\Phi = \Phi^H[\mathcal{T}]$, where $\mathcal{T} \in \mathbb{R}^{n \times n \times n_3}$ with each frontal slice being the $n \times n$ identity matrix.

Definition 4 [23, Definition 5.1] A tensor $\mathcal{Q} \in \mathbb{C}^{n \times n \times n_3}$ is unitary with respect to Φ -product if it satisfies

$$\mathcal{Q}^H \diamond_\Phi \mathcal{Q} = \mathcal{Q} \diamond_\Phi \mathcal{Q}^H = \mathcal{I}_\Phi,$$

where \mathcal{I}_Φ is the identity tensor.

Definition 5 The inner product of $\mathcal{A}, \mathcal{B} \in \mathbb{C}^{n_1 \times n_2 \times n_3}$ is defined as

$$\langle \mathcal{A}, \mathcal{B} \rangle = \sum_{i=1}^{n_3} \langle \mathcal{A}^{(i)}, \mathcal{B}^{(i)} \rangle = \langle \bar{\mathcal{A}}_\Phi, \bar{\mathcal{B}}_\Phi \rangle. \quad (2.2)$$

In the above definition, $\langle \mathcal{A}^{(i)}, \mathcal{B}^{(i)} \rangle$ is the standard inner product of two matrices. In addition, a tensor \mathcal{A} is called to be diagonal if each frontal slice $\mathcal{A}^{(i)}$ is a diagonal matrix [25]. Based on the above definitions, we have the following transformed tensor SVD with respect to Φ .

Theorem 1 [23, Theorem 5.1] Suppose that $\mathcal{A} \in \mathbb{C}^{n_1 \times n_2 \times n_3}$. Then \mathcal{A} can be factorized as follows:

$$\mathcal{A} = \mathcal{U} \diamond_\Phi \mathcal{S} \diamond_\Phi \mathcal{V}^H, \quad (2.3)$$

where $\mathcal{U} \in \mathbb{C}^{n_1 \times n_1 \times n_3}$, $\mathcal{V} \in \mathbb{C}^{n_2 \times n_2 \times n_3}$ are unitary tensors with respect to Φ -product, and $\mathcal{S} \in \mathbb{C}^{n_1 \times n_2 \times n_3}$ is a diagonal tensor.

The tensors \mathcal{U} , \mathcal{V} and \mathcal{S} in the transformed tensor SVD can be computed by SVDs of $\hat{\mathcal{A}}_\Phi^{(i)}$, which is summarized in Algorithm 1.

Algorithm 1 Transformed tensor SVD for third-order tensors [23]

Input: $\mathcal{A} \in \mathbb{C}^{n_1 \times n_2 \times n_3}$.

1: $\hat{\mathcal{A}} = \Phi[\mathcal{A}]$;

2: **for** $i = 1, \dots, n_3$ **do**

3: $[\mathbf{U}, \mathbf{S}, \mathbf{V}] = \text{SVD}(\hat{\mathcal{A}}^{(i)})$;

4: $\hat{\mathcal{U}}^{(i)} = \mathbf{U}$, $\hat{\mathcal{S}}^{(i)} = \mathbf{S}$, $\hat{\mathcal{V}}^{(i)} = \mathbf{V}$;

5: **end for**

6: $\mathcal{U} = \Phi^H[\hat{\mathcal{U}}]$, $\mathcal{S} = \Phi^H[\hat{\mathcal{S}}]$, $\mathcal{V} = \Phi^H[\hat{\mathcal{V}}]$.

Output: $\mathcal{U} \in \mathbb{C}^{n_1 \times n_1 \times n_3}$, $\mathcal{S} \in \mathbb{C}^{n_1 \times n_2 \times n_3}$, $\mathcal{V} \in \mathbb{C}^{n_2 \times n_2 \times n_3}$.

Remark 2.1 For computational improvement, we also use the skinny transformed tensor SVD. For any $\mathcal{A} \in \mathbb{C}^{n_1 \times n_2 \times n_3}$ with $\text{rank}(\mathcal{A}) = r$ (see in the following definition), the skinny transformed tensor SVD is given by $\mathcal{A} = \mathcal{U} \diamond_\Phi \mathcal{S} \diamond_\Phi \mathcal{V}^H$, where $\mathcal{U} \in \mathbb{C}^{n_1 \times r \times n_3}$, $\mathcal{V} \in \mathbb{C}^{n_2 \times r \times n_3}$ are unitary tensors with respect to Φ -product, and $\mathcal{S} \in \mathbb{C}^{r \times r \times n_3}$ is a diagonal tensor.

Based on the transformed tensor SVD given in Theorem 1, the tensor tubal rank can be defined as follows.

Definition 6 The tubal multi-rank of a tensor $\mathcal{A} \in \mathbb{C}^{n_1 \times n_2 \times n_3}$ is a vector $\mathbf{r} \in \mathbb{R}^{n_3}$ with its i -th entry being the rank of the i -th frontal slice of $\hat{\mathcal{A}}_{\Phi}$, i.e., $r_i = \text{rank}(\hat{\mathcal{A}}_{\Phi}^{(i)})$. The tensor tubal rank, denoted as $\text{rank}(\mathcal{A})$, is defined as the number of nonzero singular tubes of \mathcal{S} , where \mathcal{S} comes from the transformed tensor SVD of $\mathcal{A} = \mathcal{U} \diamond_{\Phi} \mathcal{S} \diamond_{\Phi} \mathcal{V}^H$, i.e.,

$$\text{rank}(\mathcal{A}) = \#\{i : \mathcal{S}(i, i, :) \neq \mathbf{0}\} = \max_i r_i. \quad (2.4)$$

It follows from [21] that the tensor spectral norm of $\mathcal{A} \in \mathbb{C}^{n_1 \times n_2 \times n_3}$ relate to Φ , denoted as $\|\mathcal{A}\|$, can be defined as $\|\mathcal{A}\| = \|\Phi[\mathcal{A}]\|$. In other words, the tensor spectral norm of \mathcal{A} equals to the matrix spectral norm of its block diagonal form in the transform domain. Moreover, suppose that a tensor operator L can be represented as a tensor \mathcal{L} via Φ -product with \mathcal{A} , we have $\|L\|_{\text{op}} = \|\mathcal{L}\|$. The aim of this paper is to recover a low transformed tubal rank tensor, which motivates us to introduce the following definition of tensor nuclear norm.

Definition 7 The transformed tubal nuclear norm of a tensor $\mathcal{A} \in \mathbb{C}^{n_1 \times n_2 \times n_3}$, denoted as $\|\mathcal{A}\|_{\text{TTNN}}$, is the sum of the nuclear norms of all the frontal slices of $\hat{\mathcal{A}}_{\Phi}$, i.e., $\|\mathcal{A}\|_{\text{TTNN}} = \sum_{i=1}^{n_3} \|\hat{\mathcal{A}}_{\Phi}^{(i)}\|_*$.

Next we show that the transformed tubal nuclear norm (TTNN) of a tensor is the convex envelope of the sum of the elements of the tensor tubal multi-rank over a unit ball of the tensor spectral norm. This is why the TTNN is useful for low transformed tubal rank tensor recovery. We remark this is the new result in the literature, and the proof is different from [12, Theorem 1] because we consider the complex-valued matrices and tensors.

Lemma 1 For any tensor $\mathcal{X} \in \mathbb{C}^{n_1 \times n_2 \times n_3}$, $\text{rank}_{\text{sum}}(\mathcal{X}) = \sum_{i=1}^{n_3} \text{rank}(\hat{\mathcal{X}}_{\Phi}^{(i)})$ denotes a transformed tubal multi-rank function. Then $\|\mathcal{X}\|_{\text{TTNN}}$ is the convex envelope of the function $\text{rank}_{\text{sum}}(\mathcal{X})$ on the set $\{\mathcal{X} \mid \|\mathcal{X}\| \leq 1\}$.

The proof can be found in Appendix A. Next we will introduce two kinds of tensor basis which play important roles in tensor coordinate decomposition as well as introducing the tensor incoherence conditions in the sequel.

Definition 8 (i) The transformed column basis with respect to Φ , denoted as \vec{e}_i , is a tensor of size $n_1 \times 1 \times n_3$ with the i -th tube of $\Phi[\vec{e}_i]$ is equal to $\vec{1}$ (each entry in the i -th tube is 1) and the rest equaling to 0. Its associated conjugate transpose \vec{e}_i^H is called transformed row basis with respect to Φ . (ii) The transformed tube basis with respect to Φ , denoted as \dot{e}_k , is a tensor of size $1 \times 1 \times n_3$ with the $(1, 1, k)$ -th entry of $\Phi[\dot{e}_k]$ equaling to 1 and the remaining entries equaling to 0.

Denote \mathcal{E}_{ijk} as a unit tensor with the (i, j, k) -th entry equaling to 1 and others equaling to 0. Based on Definition 8, \mathcal{E}_{ijk} can be expressed as

$$\mathcal{E}_{ijk} = \Phi[\vec{e}_i \diamond_{\Phi} \dot{e}_k \diamond_{\Phi} \vec{e}_j]. \quad (2.5)$$

Then for a third-order tensor $\mathcal{A} \in \mathbb{C}^{n_1 \times n_2 \times n_3}$, we can decompose it as

$$\mathcal{A} = \sum_{i,j,k} \langle \mathcal{E}_{ijk}, \mathcal{A} \rangle \mathcal{E}_{ijk} = \sum_{i,j,k} \mathcal{A}_{ijk} \mathcal{E}_{ijk}. \quad (2.6)$$

These properties will be used many times in the proof of our main results in Section 3. These new bases are different from existing bases and they are required in the proof of unitary transform-based tensor recovery.

3 Recovery Results by Transformed Tensor SVD

Suppose that we are given a third-order tensor \mathcal{L}_0 that has a low transformed tubal rank with respect to Φ and is also corrupted by a sparse tensor \mathcal{E}_0 , where the transformed tubal rank of \mathcal{L}_0 is not known. Moreover, we have no idea about the locations of the nonzero entries of \mathcal{E}_0 , not even how many there are. We would like to recover \mathcal{L}_0 from a set of observed entries of \mathcal{X} . We use the TTNN of a tensor to get a low rank solution and ℓ_1 norm to get a sparse solution. Mathematically, the model can be stated as follows:

$$\min_{\mathcal{L}, \mathcal{E}} \|\mathcal{L}\|_{\text{TTNN}} + \lambda \|\mathcal{E}\|_1, \quad \text{s.t.}, \quad \mathcal{P}_\Omega(\mathcal{L} + \mathcal{E}) = \mathcal{P}_\Omega(\mathcal{X}), \quad (3.7)$$

where λ is a penalty parameter and \mathcal{P}_Ω is a linear projection such that the entries in the set Ω are given while the remaining entries are missing.

We remark that the convex optimization problems constructed in [21, 52, 53] can be seen as special cases of (3.7), which aim to solve the tensor completion and tensor robust principal component analysis, respectively. For instance, if the unitary transform Φ is based on discrete Fourier transform, the transformed tubal nuclear norm can be replaced by the tubal nuclear norm (TNN).

Here we need some incoherence conditions on \mathcal{L}_0 to ensure that it is not sparse.

Definition 9 Assume that $\text{rank}(\mathcal{L}_0) = r$ and its skinny transformed tensor SVD is $\mathcal{L}_0 = \mathcal{U} \diamond_\Phi \mathcal{S} \diamond_\Phi \mathcal{V}^H$. \mathcal{L}_0 is said to satisfy the transformed tensor incoherence conditions with parameter $\mu > 0$ if

$$\max_{i=1, \dots, n_1} \|\mathcal{U}^H \diamond_\Phi \vec{e}_i\|_F \leq \sqrt{\frac{\mu r}{n_1}}, \quad (3.8)$$

$$\max_{j=1, \dots, n_2} \|\mathcal{V}^H \diamond_\Phi \vec{e}_j\|_F \leq \sqrt{\frac{\mu r}{n_2}}, \quad (3.9)$$

and

$$\|\mathcal{U} \diamond_\Phi \mathcal{V}^H\|_\infty \leq \sqrt{\frac{\mu r}{n_1 n_2 n_3}}, \quad (3.10)$$

where \vec{e}_i and \vec{e}_j are the tensor basis with respect to Φ .

For convenience, we denote $n_{(1)} = \max(n_1, n_2)$ and $n_{(2)} = \min(n_1, n_2)$. The main result of this paper can be stated in the following theorem.

Theorem 2 Suppose that $\mathcal{L}_0 \in \mathbb{C}^{n_1 \times n_2 \times n_3}$ obeys (3.8)-(3.10), and the observation set Ω is uniformly distributed among all sets of cardinality $m = \rho n_1 n_2 n_3$. Also suppose that each observed entry is independently corrupted with probability γ . Then, there exist universal constants $c_1, c_2 > 0$ such that with probability at least $1 - c_1(n_{(1)} n_3)^{-c_2}$, the recovery of \mathcal{L}_0 with $\lambda = 1/\sqrt{\rho n_{(1)} n_3}$ is exact, provided that

$$r \leq \frac{c_r n_{(2)}}{\mu (\log(n_{(1)} n_3))^2} \quad \text{and} \quad \gamma \leq c_\gamma, \quad (3.11)$$

where c_r and c_γ are two positive constants.

Remark 3.1 By the inner product given in Definition 5, a direct generalization of the transformed tensor incoherence conditions listed in [21] for arbitrary unitary transform are

$$\max_{i=1, \dots, n_1} \|\mathcal{U}^H \diamond_\Phi \vec{e}_i\|_F \leq \sqrt{\frac{\mu r}{n_1 n_3}}, \quad \max_{j=1, \dots, n_2} \|\mathcal{V}^H \diamond_\Phi \vec{e}_j\|_F \leq \sqrt{\frac{\mu r}{n_2 n_3}},$$

and

$$\|\mathcal{U} \diamond_{\Phi} \mathcal{V}^H\|_{\infty} \leq \sqrt{\frac{\mu r}{n_1 n_2 n_3^2}}.$$

The right hands of the three inequalities are obviously smaller than those given in (3.8)-(3.10), which means that the exact recovery conditions are weaker than those of [21].

The idea of the proof is to employ convex analysis to derive the conditions in which one can check whether the pair $(\mathcal{L}, \mathcal{E})$ is the unique minimizer to (3.7), and to explicitly show that the conditions in Theorem 2 are met with overwhelming probability. The main tools of our proof are the non-commutative Bernstein Inequality (NBI) and the golfing scheme [4, 15]. The detailed proof is given in Appendix B.

3.1 Optimization Algorithm

In this subsection, we develop a symmetric Gauss-Seidel based multi-block alternating direction method of multipliers (sGS-ADMM) [6, 28] to solve the robust tensor completion problem (3.7). The sGS-ADMM has been validated the efficiency in many fields, e.g., see [1, 6, 28, 46, 51] and references therein. Let $\mathcal{L} + \mathcal{E} = \mathcal{M}$. Problem (3.7) can be rewritten as

$$\begin{aligned} \min_{\mathcal{L}, \mathcal{E}, \mathcal{M}} \quad & \|\mathcal{L}\|_{\text{TTNN}} + \lambda \|\mathcal{E}\|_1 \\ \text{s.t.} \quad & \mathcal{L} + \mathcal{E} = \mathcal{M}, \mathcal{P}_{\Omega}(\mathcal{M}) = \mathcal{P}_{\Omega}(\mathcal{X}). \end{aligned} \quad (3.12)$$

The augmented Lagrangian function of (3.12) is defined by

$$L(\mathcal{L}, \mathcal{E}, \mathcal{M}, \mathcal{Z}) := \|\mathcal{L}\|_{\text{TTNN}} + \lambda \|\mathcal{E}\|_1 - \langle \mathcal{Z}, \mathcal{L} + \mathcal{E} - \mathcal{M} \rangle + \frac{\beta}{2} \|\mathcal{L} + \mathcal{E} - \mathcal{M}\|_F^2,$$

where \mathcal{Z} is the Lagrangian multiplier and β is the penalty parameter. Let $\mathfrak{D} := \{\mathcal{M} \in \mathbb{C}^{n_1 \times n_2 \times n_3} : \mathcal{P}_{\Omega}(\mathcal{M}) = \mathcal{P}_{\Omega}(\mathcal{X})\}$. The iteration system of the sGS-ADMM can be described as follows:

$$\mathcal{M}^{k+\frac{1}{2}} = \arg \min_{\mathcal{M} \in \mathfrak{D}} \left\{ L(\mathcal{L}^k, \mathcal{E}^k, \mathcal{M}, \mathcal{Z}^k) \right\}, \quad (3.13)$$

$$\mathcal{L}^{k+1} = \arg \min_{\mathcal{L}} \left\{ L(\mathcal{L}, \mathcal{E}^k, \mathcal{M}^{k+\frac{1}{2}}, \mathcal{Z}^k) \right\}, \quad (3.14)$$

$$\mathcal{M}^{k+1} = \arg \min_{\mathcal{M} \in \mathfrak{D}} \left\{ L(\mathcal{L}^{k+1}, \mathcal{E}^k, \mathcal{M}, \mathcal{Z}^k) \right\}, \quad (3.15)$$

$$\mathcal{E}^{k+1} = \arg \min_{\mathcal{E}} \left\{ L(\mathcal{L}^{k+1}, \mathcal{E}, \mathcal{M}^{k+1}, \mathcal{Z}^k) \right\}, \quad (3.16)$$

$$\mathcal{Z}^{k+1} = \mathcal{Z}^k - \tau \beta (\mathcal{L}^{k+1} + \mathcal{E}^{k+1} - \mathcal{M}^{k+1}), \quad (3.17)$$

where $\tau \in (0, (1 + \sqrt{5})/2)$ is the step-length.

The solution with respect to \mathcal{M} can be given by

$$\mathcal{M} = \begin{cases} \mathcal{X}_{ijk}, & \text{if } (i, j, k) \in \Omega, \\ \left(\mathcal{L} + \mathcal{E} - \frac{1}{\beta} \mathcal{Z} \right)_{ijk}, & \text{otherwise.} \end{cases} \quad (3.18)$$

Similar to the proximal mapping of the nuclear norm of a matrix, we give the proximal mapping of the TTNN of a tensor. The proximal mapping of $\|\cdot\|_{\text{TTNN}}$ at \mathcal{Y} can be given in the following theorem.

Theorem 3 For any $\mathcal{Y} = \mathcal{U} \diamond_{\Phi} \mathcal{S} \diamond_{\Phi} \mathcal{V}^H$, the minimizer of the following problem

$$\min_{\mathcal{X}} \left\{ \lambda \|\mathcal{X}\|_{\text{TTNN}} + \frac{1}{2} \|\mathcal{X} - \mathcal{Y}\|_F^2 \right\} \quad (3.19)$$

is given by

$$\text{Prox}_{\lambda \|\cdot\|_{\text{TTNN}}}(\mathcal{Y}) := \mathcal{U} \diamond_{\Phi} \mathcal{S}_{\lambda} \diamond_{\Phi} \mathcal{V}^H, \quad (3.20)$$

where $\mathcal{S}_{\lambda} = \Phi^H[\hat{\mathcal{S}}_{\lambda}]$ and $\hat{\mathcal{S}}_{\lambda} = \max\{\hat{\mathcal{S}}_{\Phi} - \lambda, 0\}$.

By the definition of the TTNN, problem (3.19) can be rewritten as

$$\min_{\mathcal{X}} \left\{ \sum_{i=1}^{n_3} \lambda \|\hat{\mathbf{X}}_{\Phi}^{(i)}\|_* + \frac{1}{2} \|\hat{\mathbf{X}}_{\Phi}^{(i)} - \hat{\mathbf{Y}}_{\Phi}^{(i)}\|_F^2 \right\} \quad (3.21)$$

By [3, Theorem 2.1], the minimizer of (3.21) is given by

$$\hat{\mathbf{X}}_{\Phi}^{(i)} = \hat{\mathbf{U}}_{\Phi}^{(i)} \hat{\Sigma}_{\lambda}(\hat{\mathbf{V}}_{\Phi}^{(i)})^H,$$

where $\hat{\Sigma}_{\lambda} = \max\{\hat{\mathbf{S}}_{\Phi}^{(i)} - \lambda, 0\}$. By using the inverse unitary transform along the third-dimension, we get that the optimal solution of (3.19) is given by (3.20).

The subproblem with respect to \mathcal{L} in (3.14) can be described as

$$\min \|\mathcal{L}\|_{\text{TTNN}} + \frac{\beta}{2} \left\| \mathcal{L} - \left(\mathcal{M}^{k+\frac{1}{2}} + \frac{1}{\beta} \mathcal{Z}^k - \mathcal{E}^k \right) \right\|_F^2. \quad (3.22)$$

By Theorem 3, the minimizer of problem (3.22) is given by

$$\mathcal{L}^{k+1} = \mathcal{U} \diamond_{\Phi} \mathcal{S}_{\beta} \diamond_{\Phi} \mathcal{V}^H, \quad (3.23)$$

where $\mathcal{M}^{k+\frac{1}{2}} + \frac{1}{\beta} \mathcal{Z}^k - \mathcal{E}^k = \mathcal{U} \diamond_{\Phi} \mathcal{S} \diamond_{\Phi} \mathcal{V}^H$ and $\mathcal{S}_{\beta} = \Phi^H[\hat{\mathcal{S}}_{\beta}]$ with $\hat{\mathcal{S}}_{\beta} = \max\{\hat{\mathcal{S}}_{\Phi} - \frac{1}{\beta}, 0\}$. The minimizer with respect to \mathcal{E} in (3.16) can be given by

$$\mathcal{E}^{k+1} = \text{sgn}(\mathcal{H}) \circ \max \left\{ |\mathcal{H}| - \frac{\lambda}{\beta}, 0 \right\}, \quad (3.24)$$

where $\mathcal{H} := \mathcal{M}^{k+1} + \frac{1}{\beta} \mathcal{Z}^k - \mathcal{L}^{k+1}$, \circ denotes the point-wise product, and $\text{sgn}(\cdot)$ denotes the signum function. i.e.,

$$\text{sgn}(y) := \begin{cases} 1, & \text{if } y > 0, \\ 0, & \text{if } y = 0, \\ -1, & \text{if } y < 0. \end{cases}$$

Since only two blocks of the objective function in (3.12) are nonsmooth and the other block is not involved in (3.12), the sGS-ADMM is convergent [28, Theorem 3]. The sGS-ADMM for solving (3.12) can be stated in Algorithm 2.

4 Experimental Results

In this section, numerical results are presented to show the effectiveness of the proposed method for robust tensor completion. We compare the transformed tensor SVD with the sum of nuclear norms of unfolding matrices of a tensor plus a sparse tensor (SNN)¹ [14], tensor SVD using Fourier transform (t-SVD (Fourier))² [31], and low-rank tensor completion by parallel matrix factorization (TMac)³ [48]. All the experiments are performed under Windows 7 and MATLAB R2018a running on a desktop (Intel Core i7, @ 3.40GHz, 8.00G RAM).

¹<https://tonyzqin.wordpress.com/>

²<https://canyilu.github.io/publications/>

³<https://xu-yangyang.github.io/TMac/>

Algorithm 2 A symmetric Gauss-Seidel based multi-block ADMM for solving (3.12)

Input: $\tau \in (0, (1 + \sqrt{5})/2)$, $\beta > 0$, $\mathcal{L}^0, \mathcal{E}^0, \mathcal{Z}^0$. For $k = 0, 1, 2, \dots$, perform the following steps:

1: Compute $\mathcal{M}^{k+\frac{1}{2}}$ by

$$\mathcal{M}^{k+\frac{1}{2}} = \begin{cases} \mathcal{X}_{ijk}, & \text{if } (i, j, k) \in \Omega, \\ \left(\mathcal{L}^k + \mathcal{E}^k - \frac{1}{\beta}\mathcal{Z}^k\right)_{ijk}, & \text{otherwise.} \end{cases}$$

2: Compute \mathcal{L}^{k+1} via (3.23).

3: Compute \mathcal{M}^{k+1} by

$$\mathcal{M}^{k+1} = \begin{cases} \mathcal{X}_{ijk}, & \text{if } (i, j, k) \in \Omega, \\ \left(\mathcal{L}^{k+1} + \mathcal{E}^k - \frac{1}{\beta}\mathcal{Z}^k\right)_{ijk}, & \text{otherwise.} \end{cases}$$

4: Compute \mathcal{E}^{k+1} via (3.24).

5: Update \mathcal{Z}^{k+1} by (3.17).

6: If a stopping criterion is not met, set $k := k + 1$ and go to step 1.

4.1 Experimental Setting

The sampling ratio of observations is defined as $\rho := \frac{|\Omega|}{n_1 n_2 n_3}$, where Ω is generated uniformly at random and $|\Omega|$ denotes the number of the entries of Ω . In order to evaluate the performance of different methods for real-world tensors, the peak signal-to-noise ratio (PSNR) is used to measure the quality of the estimated tensors, which is defined as follows:

$$\text{PSNR} := 10 \log_{10} \frac{n_1 n_2 n_3 (\mathcal{L}_{\max} - \mathcal{L}_{\min})^2}{\|\mathcal{L} - \mathcal{L}_0\|_F^2},$$

where \mathcal{L} is the recovered solution, \mathcal{L}_0 is the ground-truth tensor, \mathcal{L}_{\max} and \mathcal{L}_{\min} are maximal and minimal entries of \mathcal{L}_0 , respectively.

As suggested by Theorem 2, we set $\lambda = \frac{a}{\sqrt{n_{(1)} n_3}}$ and adjust it slightly to obtain the best possible results. In all experiments, a is selected from $\{1.1, 1.3, 1.7, 1.8, 2\}$ in Fourier transform and from $\{10, 15, 18, 20, 23, 25, 28, 30, 33, 35, 40, 45, 50\}$ in unitary and wavelet transforms. Moreover, τ is set to be 1.618 for its convergence [28] and β is chosen from $\{0.01, 0.05, 0.1, 0.5\}$ to get the highest PSNR values in Algorithm 2. The Karush-Kuhn-Tucker (KKT) conditions of problem (3.12) are given by

$$\begin{cases} \mathcal{Z} \in \partial\|\mathcal{L}\|_{\text{TTNN}}, \mathcal{Z} \in \partial\lambda\|\mathcal{E}\|_1, \\ \mathcal{L} + \mathcal{E} = \mathcal{M}, \mathcal{P}_\Omega(\mathcal{M}) = \mathcal{P}_\Omega(\mathcal{X}), \end{cases}$$

where $\partial\|\mathcal{L}\|_{\text{TTNN}}$ and $\partial\lambda\|\mathcal{E}\|_1$ denote the subdifferentials of $\|\cdot\|_{\text{TTNN}}$ and $\lambda\|\cdot\|_1$, respectively. Note that $\mathcal{P}_\Omega(\mathcal{M}) = \mathcal{P}_\Omega(\mathcal{X})$ is always satisfied in each iteration of the sGS-ADMM. We measure the accuracy of an approximate optimal solution by using the following relative KKT residual:

$$\eta_{res} := \max\{\eta_z, \eta_e, \eta_m\},$$

where

$$\eta_z = \frac{\|\mathcal{L} - \text{Prox}_{\|\cdot\|_{\text{TTNN}}}(\mathcal{Z} + \mathcal{L})\|_F}{1 + \|\mathcal{Z}\|_F + \|\mathcal{L}\|_F}, \eta_e = \frac{\|\mathcal{E} - \text{Prox}_{\lambda\|\cdot\|_1}(\mathcal{Z} + \mathcal{E})\|_F}{1 + \|\mathcal{Z}\|_F + \|\mathcal{E}\|_F},$$

$$\eta_m = \frac{\|\mathcal{L} + \mathcal{E} - \mathcal{M}\|_F}{1 + \|\mathcal{L}\|_F + \|\mathcal{E}\|_F + \|\mathcal{M}\|_F}.$$

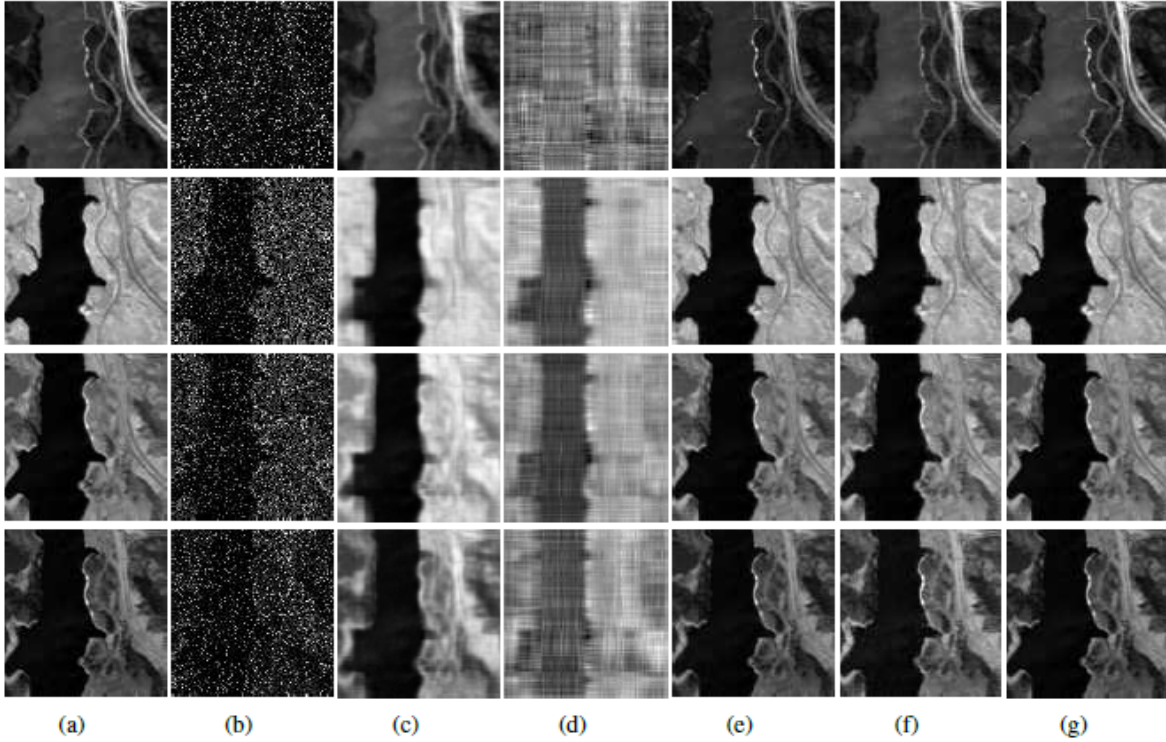


Figure 4.1: (a) Original images for Japsen Ridge dataset; (b) Observed images (60% sampling ratio and 30% corrupted entries); (c) Recovered images by SNN [PSNR = 26.00]; (d) Recovered images by TMac [PSNR = 16.47]; (e) Recovered images by t-SVD (Fourier) [PSNR = 33.63]; (f) Recovered images by t-SVD (wavelet) [PSNR = 33.59]; (g) Recovered images by t-SVD (data) [PSNR = 37.38].

Here Prox_g is the proximal mapping of g , i.e., $\text{Prox}_g(y) = \arg \min_x \{g(x) + \frac{1}{2}\|x - y\|^2\}$. The stopping criterion of the Algorithm is set to $\eta_{res} \leq 5 \times 10^{-4}$ and the maximum number of iterations is set to be 500.

For the sparse level of \mathcal{E} , a fraction γ of its entries are uniformly corrupted by additive independent and identically distributed noise from a standard Gaussian distribution $N(0, 1)$ at random, which generates the sparse tensor \mathcal{E} . The testing real-world tensors are rescaled in $[0, 1]$.

In the following test, we consider two different kinds of transformations in the proposed method. The first one is a Daubechies 4 (db4) discrete wavelet transform in the periodic mode [10] to compute transformed tensor SVD (called t-SVD (wavelet)). The second one is based on data to construct a unitary transform matrix. We note that \mathcal{A} is unfolded into a matrix \mathbf{A} along the third-dimension (called t-SVD (data)). Then we take the singular value decomposition of the unfolding matrix $\mathbf{A} = \mathbf{U}\mathbf{\Sigma}\mathbf{V}^H$. It is interesting to see that \mathbf{U}^H is the optimal transformation to obtain a low rank matrix of \mathbf{A} :

$$\min_{\text{rank}(\mathbf{B})=k, \text{unitary } \Phi} \|\Phi\mathbf{A} - \mathbf{B}\|_F^2.$$

In practice, the initial estimator \mathcal{A} in the robust tensor completion problem by using the Fourier transform (i.e., t-SVD completion method) can be used to generate Φ .

4.2 Hyperspectral Data

In this subsection, we use three hyperspectral datasets: Samson, Japsen Ridge, and Urban datasets [55] to show the effectiveness of the proposed method. The testing datasets are third-order tensors (length

Table 4.1: PSNR values obtained by SNN, TMac, t-SVD (Fourier), t-SVD (wavelet), and t-SVD (data) for hyperspectral datasets. The boldface number is the best and the underline number is the second best.

	ρ	γ	SNN	TMac	t-SVD (Fourier)	t-SVD (wavelet)	t-SVD (data)
Samson	0.6	0.1	30.22	23.15	38.53	<u>45.43</u>	53.30
		0.2	29.63	19.35	34.80	<u>41.29</u>	50.68
		0.3	28.06	16.82	32.26	<u>38.22</u>	45.87
	0.8	0.1	32.43	23.28	40.87	<u>47.34</u>	54.40
		0.2	30.84	19.42	36.82	<u>44.69</u>	52.49
		0.3	29.35	16.86	33.58	<u>39.46</u>	48.28
Japsen Ridge	0.6	0.1	30.13	21.73	39.22	<u>40.60</u>	45.13
		0.2	27.92	18.76	36.38	<u>37.20</u>	41.13
		0.3	26.00	16.47	<u>33.63</u>	<u>33.59</u>	37.38
	0.8	0.1	31.98	21.84	40.78	<u>42.64</u>	46.76
		0.2	29.61	18.81	37.88	<u>38.87</u>	43.13
		0.3	27.49	16.51	35.15	<u>35.81</u>	39.33
Urban	0.6	0.1	27.88	22.20	38.78	<u>39.10</u>	47.76
		0.2	26.13	18.43	<u>36.08</u>	<u>35.70</u>	44.51
		0.3	24.69	16.06	<u>33.39</u>	<u>32.16</u>	39.63
	0.8	0.1	30.31	22.29	40.76	<u>42.94</u>	49.76
		0.2	27.89	18.45	37.77	<u>38.44</u>	45.98
		0.3	26.06	16.07	<u>34.98</u>	<u>33.37</u>	42.26

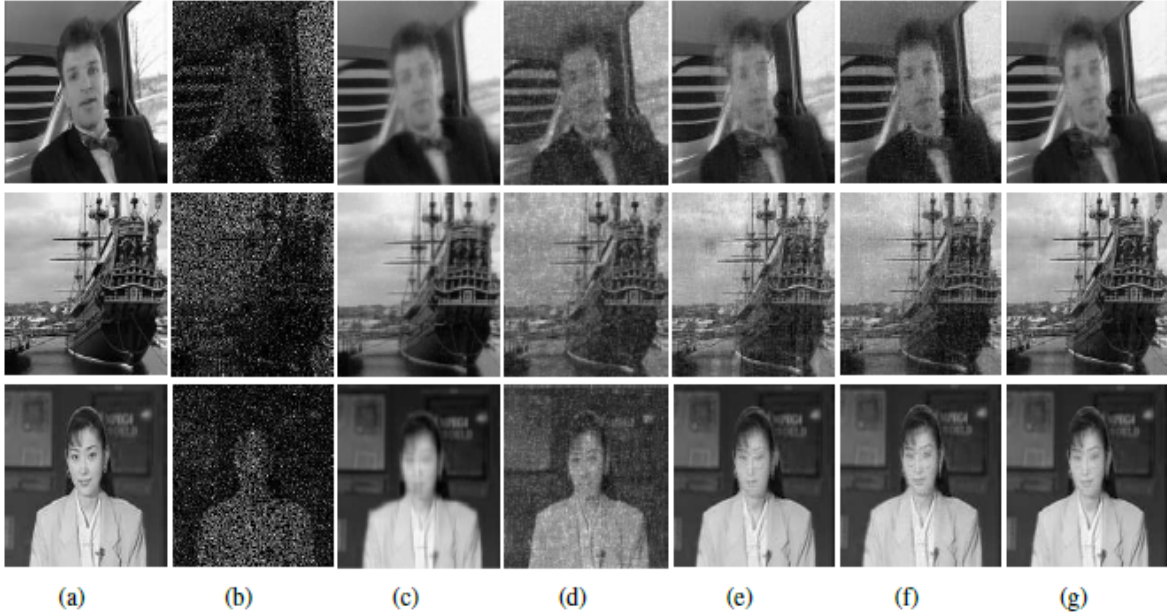


Figure 4.2: Recovered images by SNN, TMac, t-SVD (Fourier), t-SVD (wavelet) and t-SVD (data) in robust tensor completion for video data with 60% sampling ratio and 20% corrupted entries. (a) Original images. (b) Observed images. (c) SNN. (d) TMac. (e) t-SVD (Fourier). (f) t-SVD (wavelet). (g) t-SVD (data).

\times width \times channels). We describe the three datasets in the following:

- For the Samson dataset, we only utilize a region of 95×95 in each image, where each pixel is recorded at 156 frequency channels covering the wavelengths from $401nm$ to $889nm$. Then the spectral resolution is highly up to $3.13nm$. Thus, the size of the resulting tensor is $95 \times 95 \times 156$.
- For the Japsen Ridge dataset, each pixel is recorded at 224 frequency channels with wavelengths being from $380nm$ to $2500nm$. The spectral resolution is up to $9.46nm$. Since this hyperspectral

Table 4.2: The PSNR values of video data by SNN, TMac, t-SVD (Fourier), t-SVD (wavelet), and t-SVD (data). The boldface number is the best and the underline number is the second best.

	ρ	γ	SNN	TMac	t-SVD (Fourier)	t-SVD (wavelet)	t-SVD (data)
Carphone	0.6	0.1	26.80	20.86	30.70	<u>31.21</u>	32.38
		0.2	24.88	17.35	<u>28.82</u>	28.30	30.14
		0.3	23.39	15.19	27.21	<u>27.32</u>	28.09
	0.8	0.1	28.74	21.03	32.57	<u>32.73</u>	34.06
		0.2	26.35	17.47	30.13	<u>30.25</u>	31.29
		0.3	24.68	15.27	28.16	28.18	29.10
Galleon	0.6	0.1	24.56	20.47	27.44	<u>29.18</u>	29.80
		0.2	22.14	17.19	25.63	<u>26.55</u>	27.55
		0.3	19.07	15.12	24.05	<u>24.26</u>	25.84
	0.8	0.1	26.86	20.75	29.37	<u>30.67</u>	31.71
		0.2	24.32	17.37	27.01	<u>28.44</u>	29.03
		0.3	22.10	15.23	25.08	<u>26.26</u>	26.93
Announcer	0.6	0.1	29.58	21.14	37.90	<u>38.24</u>	39.44
		0.2	27.55	17.52	<u>35.35</u>	35.07	36.57
		0.3	26.36	15.33	<u>33.02</u>	31.94	34.14
	0.8	0.1	31.57	21.24	39.62	<u>40.45</u>	41.28
		0.2	28.67	17.58	<u>36.61</u>	35.91	37.97
		0.3	27.50	15.37	<u>34.15</u>	33.54	35.23

image is too complex to get the ground truth, a subimage of 100×100 pixels is considered. The first pixel starts from the (105, 269)th pixel in the original image. Due to dense water vapor and atmospheric effects, we only remain 198 channels. Therefore, the size of the resulting tensor is $100 \times 100 \times 198$.

- For the Urban dataset, there are 307×307 pixels of each image, each of which corresponds to a $2 \times 2 m^2$ area. In this image, there are 210 wavelengths ranging from $400nm$ to $2500nm$, which results in a spectral resolution of $10nm$. 162 channels of this dataset is remained due to dense water vapor and atmospheric effects. Hence, the size of the resulting tensor is $307 \times 307 \times 162$.

We consider robust tensor completion problem for the testing hyperspectral data with different sampling ratios and γ . Figure 4.1 displays the visual comparisons of different methods for the Japser Ridge dataset with 60% sampling ratio and 30% corruption entries. We can observe that the visual quality obtained by t-SVD (data) is better than that obtained by SNN, TMac, t-SVD (Fourier), and t-SVD (wavelet). The PSNR values obtained by different methods are displayed in Table 4.1. We can observe that the PSNR values obtained by t-SVD (data) are much higher than those obtained by SNN, TMac, t-SVD, and t-SVD (wavelet) for different sampling ratios (0.6, 0.8) and γ (0.1, 0.2, 0.3). The improvements of t-SVD (data) are very impressive, especially for small γ . The performance of t-SVD (wavelet) is better than that of SNN, TMac, and t-SVD (Fourier) in terms of PSNR values for the Samson and Japser Ridge datasets. For the Urban dataset, the PSNR values obtained by t-SVD (Fourier) are slightly higher than those by t-SVD (wavelet), especially for large γ .

4.3 Video Data

In this subsection, we present three video data (length \times width \times frames) including Carphone ($144 \times 176 \times 180$), Galleon ($144 \times 176 \times 200$), and Announcer ($144 \times 176 \times 200$)⁴ to show the effectiveness of the proposed method in robust tensor completion problem, where the first channels of all frames in the original data are used. We just choose 180 and 200 frames for these videos to improve the computational time.

⁴<https://media.xiph.org/video/derf/>

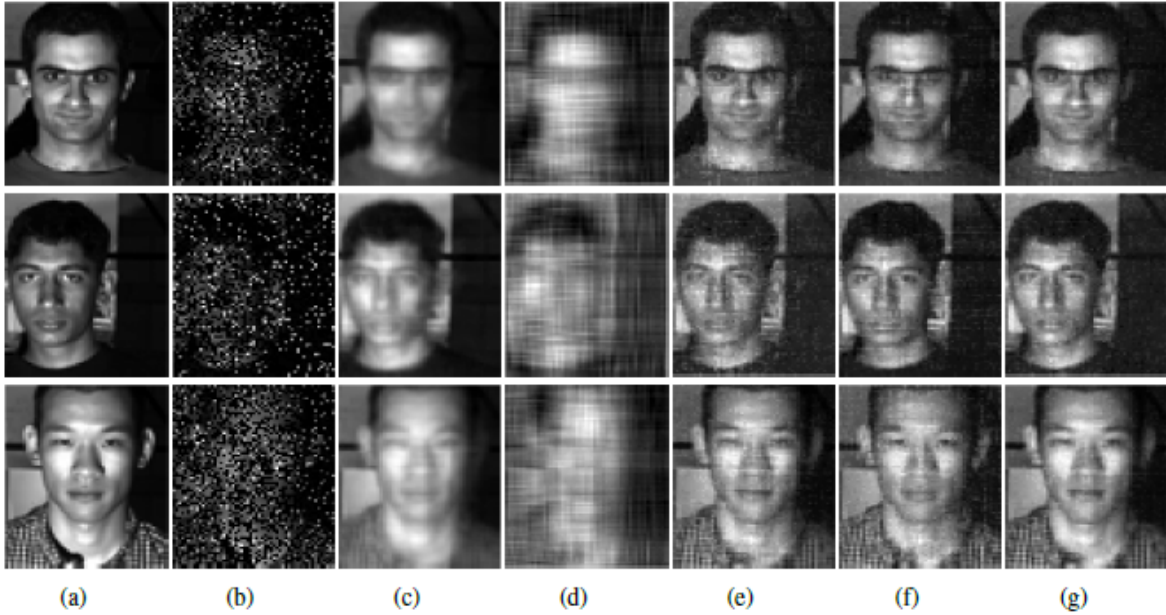


Figure 4.3: Recovered images by SNN, TMac, t-SVD (Fourier), t-SVD (wavelet), and t-SVD (data) in robust tensor completion for the extended Yale face database B with 60% sampling ratio and 20% corrupted entries. (a) Original images. (b) Observed images. (c) SNN. (d) TMac. (e) t-SVD (Fourier). (f) t-SVD (wavelet). (g) t-SVD (data).

We display the visual comparisons of the testing data in robust tensor completion with 60% sampling ratio and 20% corruption entries by SNN, TMac, t-SVD (Fourier), t-SVD (wavelet), and t-SVD (data) in Figure 4.2. We can see that the images recovered by t-SVD (data) are better than those recovered by SNN, TMac, t-SVD (Fourier), and t-SVD (wavelet) in terms of visual quality. The t-SVD (data) can keep more details than SNN, TMac, t-SVD (Fourier), and t-SVD (wavelet) for the three testing videos.

We also show the PSNR values obtained by SNN, TMac, t-SVD (Fourier), t-SVD (wavelet), and t-SVD (data) for the Carphone, Galleon and Announcer data with different sampling ratios (0.6, 0.8) and γ (0.1, 0.1, 0.3) in Table 4.2. It can be seen that the PSNR values obtained by t-SVD (data) are higher than those by SNN, TMac, t-SVD (Fourier), and t-SVD (wavelet). The PSNR values obtained by t-SVD (data) can be improved around 2dB compared with those by t-SVD (Fourier) for these data. For the Carphone and Galleon videos, the performance of t-SVD (wavelet) is better than that of t-SVD (Fourier) in terms of PSNR values. While the PSNR values obtain by t-SVD (Fourier) is slightly higher than those obtained by SNN, TMac, and t-SVD (wavelet) for large γ such as 0.2 and 0.3 cases.

4.4 Face Data

In this subsection, we use the extended Yale face database B⁵ to test the robust tensor completion problem. To improve the computational time, we crop the original image to contain the face and resize it to 73×55 . Moreover, we only choose first 30 subjects and 25 illuminations in our test. Then the size of the testing tensor is $73 \times 55 \times 750$.

The visual comparisons of SNN, TMac, t-SVD (Fourier), t-SVD (wavelet), and t-SVD (data) for the extended Yale face database B are show in Figure 4.3, where the sampling ratio is 0.6 and $\gamma = 0.2$.

⁵<http://vision.ucsd.edu/~iskwak/ExtYaleDatabase/ExtYaleB.html>

Table 4.3: The PSNR values of face data by SNN, TMac, t-SVD (Fourier), t-SVD (wavelet), and t-SVD (data). The boldface number is the best and the underline number is the second best.

ρ	γ	SNN	TMac	t-SVD (Fourier)	t-SVD (wavelet)	t-SVD (data)
0.6	0.1	24.57	19.51	26.00	<u>26.85</u>	28.76
	0.2	22.89	17.60	24.06	<u>24.73</u>	26.26
	0.3	21.76	15.77	22.22	<u>22.97</u>	23.75
0.8	0.1	26.59	19.54	28.07	<u>28.86</u>	30.67
	0.2	24.53	17.79	25.54	<u>26.02</u>	27.60
	0.3	23.06	15.93	23.59	<u>24.14</u>	25.29

It can be seen that the images obtained by t-SVD (data) are more clear than those obtained by SNN, TMac, t-SVD (Fourier), and t-SVD (wavelet).

In Table 4.3, we show the PSNR values of different sampling ratios (0.6, 0.8) and γ (0.1, 0.2, 0.3) for the extended Yale face database B in the robust tensor completion. It can be seen that the PSNR values obtained by t-SVD (data) are higher than those obtained by SNN, TMac, t-SVD (Fourier), and t-SVD (wavelet) for these sampling ratios and γ . The PSNR values of t-SVD (data) can be improved around 2dB than those of t-SVD (Fourier).

5 Concluding Remarks

We have studied the robust tensor completion problems by using transformed tensor SVD, which employs other unitary transform matrices instead of discrete Fourier transform matrix. The algebraic structure of the associated tensor product between two tensors is not necessary to be known in general and the tensor product can be defined via the unitary transform directly. With this generalized tensor product, we have shown that one can recover a low transformed tubal rank tensor exactly with overwhelming probability provided that its rank is sufficiently small and its corrupted entries are reasonably sparse. Moreover, we have proposed an “optimal” data-dependent transform method in robust tensor completion problem for third-order tensors. Numerical examples on many real-world tensors show the usefulness of the transformed tensor SVD method with wavelet and data-dependent transforms, and demonstrate that the performance of the proposed method is better than that of existing tensor completion methods.

Appendix A. Proof of Lemma 1

For convenience, we denote $\Upsilon(\mathcal{X}) = \text{rank}_{\text{sum}}(\mathcal{X})$, and $n_{(2)} = \min(n_1, n_2)$. If the spectral norm of \mathcal{X} is less than or equal to 1, the conjugate of transformed tubal multi-rank function $\Upsilon(\mathcal{X})$ on a unit ball of the tensor spectral norm can be defined as

$$\Upsilon^\sharp(\mathcal{Y}) = \sup_{\|\mathcal{X}\| \leq 1} (\text{Re}(\langle \mathcal{Y}, \mathcal{X} \rangle) - \text{rank}_{\text{sum}}(\mathcal{X})).$$

Then by the von Neumann’s theorem and the tensor inner product given in Definition 5, we can get

$$\text{Re}(\langle \mathcal{Y}, \mathcal{X} \rangle) = \text{Re}(\langle \hat{\mathcal{Y}}_\Phi, \hat{\mathcal{X}}_\Phi \rangle) = \sum_{i=1}^{n_3} \text{Re} \left(\text{Tr} \left((\hat{\mathcal{Y}}_\Phi^{(i)})^H \times \hat{\mathcal{X}}_\Phi^{(i)} \right) \right) \leq \sum_{i=1}^{n_{(2)}n_3} \sigma_i(\bar{\mathcal{Y}}_\Phi) \sigma_i(\bar{\mathcal{X}}_\Phi), \quad (5.25)$$

where $\sigma_i(\bar{\mathcal{X}}_\Phi)$ denotes the i -th largest singular value of $\bar{\mathcal{X}}_\Phi$. Let $\mathcal{Y} = \mathcal{U}_\mathcal{Y} \diamond_\Phi \Sigma_\mathcal{Y} \diamond_\Phi \mathcal{V}_\mathcal{Y}^H$ and $\mathcal{X} = \mathcal{U}_\mathcal{X} \diamond_\Phi \Sigma_\mathcal{X} \diamond_\Phi \mathcal{V}_\mathcal{X}^H$. Since $\|\mathcal{X}\| \leq 1$, we can choose $\mathcal{U}_\mathcal{X} = \mathcal{U}_\mathcal{Y}$ and $\mathcal{V}_\mathcal{X} = \mathcal{V}_\mathcal{Y}$. Thus

$$\begin{aligned} \text{Re}(\langle \mathcal{Y}, \mathcal{X} \rangle) &= \sum_{i=1}^{n_3} \text{Re}(\text{Tr}((\hat{\mathcal{Y}}_\Phi^{(i)})^H \times \hat{\mathcal{X}}_\Phi^{(i)})) \\ &= \text{Re}\left(\text{Tr}\left(\bar{\mathcal{V}}_\mathcal{Y} \times \bar{\Sigma}_\mathcal{Y} \times \bar{\mathcal{U}}_\mathcal{Y}^H \times \bar{\mathcal{U}}_\mathcal{Y} \times \bar{\Sigma}_\mathcal{X} \times \bar{\mathcal{V}}_\mathcal{Y}^H\right)\right) \\ &= \text{Re}\left(\text{Tr}\left(\bar{\mathcal{V}}_\mathcal{Y} \times \bar{\Sigma}_\mathcal{Y} \times \bar{\Sigma}_\mathcal{X} \times \bar{\mathcal{V}}_\mathcal{Y}^H\right)\right) \\ &= \sum_{i=1}^{n_{(2)}n_3} \sigma_i(\bar{\mathcal{Y}}_\Phi) \sigma_i(\bar{\mathcal{X}}_\Phi), \end{aligned}$$

which shows that the equality in (5.25) can be obtained. Therefore, the conjugate of transformed tubal multi-rank function can be rewritten as

$$\Upsilon^\#(\mathcal{Y}) = \sup_{\|\mathcal{X}\| \leq 1} \left(\sum_{i=1}^{n_{(2)}n_3} \sigma_i(\bar{\mathcal{Y}}_\Phi) \sigma_i(\bar{\mathcal{X}}_\Phi) - \text{rank}_{\text{sum}}(\mathcal{X}) \right). \quad (5.26)$$

Now we first consider separated cases with the $\text{rank}_{\text{sum}}(\mathcal{X})$ being from 0 to $n_{(2)}n_3$. If $\text{rank}_{\text{sum}}(\mathcal{X}) = 0$, then $\Upsilon^\#(\mathcal{Y}) = 0$ for all \mathcal{Y} . If $\text{rank}_{\text{sum}}(\mathcal{X}) = r$, then

$$\Upsilon^\#(\mathcal{Y}) = \max \left\{ 0, \sigma_1(\bar{\mathcal{Y}}_\Phi) - 1, \dots, \sum_{i=1}^r \sigma_i(\bar{\mathcal{Y}}_\Phi) - r, \dots, \sum_{i=1}^{n_{(2)}n_3} \sigma_i(\bar{\mathcal{Y}}_\Phi) - n_{(2)}n_3 \right\}.$$

for $1 \leq r \leq n_{(2)}n_3$. Furthermore, if $\sigma_i(\bar{\mathcal{Y}}_\Phi) - 1 > 0$, the right hand of (5.26) would be larger. Thus

$$\Upsilon^\#(\mathcal{Y}) = \begin{cases} 0, & \text{if } \|\bar{\mathcal{Y}}_\Phi\| \leq 1, \\ \sum_{i=1}^q \sigma_i(\bar{\mathcal{Y}}_\Phi) - q, & \text{if } \sigma_q(\bar{\mathcal{Y}}_\Phi) > 1 \text{ and } \sigma_{q+1}(\bar{\mathcal{Y}}_\Phi) < 1, 1 \leq q \leq r. \end{cases}$$

The conjugate of $\Upsilon^\#(\mathcal{Y})$ is defined as

$$\Upsilon^{\#\#}(\mathcal{Z}) = \sup_{\mathcal{Y}} \left(\text{Re}(\langle \mathcal{Z}, \mathcal{Y} \rangle) - \Upsilon^\#(\mathcal{Y}) \right) = \sup_{\bar{\mathcal{Y}}_\Phi} \left(\text{Tr}((\bar{\mathcal{Z}}_\Phi)^H \bar{\mathcal{Y}}_\Phi) - \Upsilon^\#(\mathcal{Y}_\Phi) \right)$$

for all $\mathcal{Z} \in \mathbb{C}^{n_1 \times n_2 \times n_3}$. In a similar vein, suppose that $\mathcal{Z} = \mathcal{U}_\mathcal{Z} \diamond_\Phi \Sigma_\mathcal{Z} \diamond_\Phi \mathcal{V}_\mathcal{Z}^H$ and $\mathcal{Y} = \mathcal{U}_\mathcal{Y} \diamond_\Phi \Sigma_\mathcal{Y} \diamond_\Phi \mathcal{V}_\mathcal{Y}^H$, by choosing $\mathcal{U}_\mathcal{Y} = \mathcal{U}_\mathcal{Z}$ and $\mathcal{V}_\mathcal{Y} = \mathcal{V}_\mathcal{Z}$, we obtain that

$$\Upsilon^{\#\#}(\mathcal{Z}) = \sup_{\mathcal{Y}} \left(\sum_{i=1}^{n_{(2)}n_3} \sigma_i(\bar{\mathcal{Z}}_\Phi) \sigma_i(\bar{\mathcal{Y}}_\Phi) - \Upsilon^\#(\mathcal{Y}) \right).$$

In the following, we can consider two cases, i.e., $\|\bar{\mathcal{Z}}_\Phi\| \geq 1$ and $\|\bar{\mathcal{Z}}_\Phi\| \leq 1$. In the first case, if $\|\bar{\mathcal{Z}}_\Phi\| \geq 1$, then $\sigma_1(\bar{\mathcal{Y}}_\Phi)$ can be chosen large enough such that

$$\begin{aligned} \Upsilon^{\#\#}(\mathcal{Z}) &= \sup_{\mathcal{Y}} \left(\sum_{i=1}^{n_{(2)}n_3} \sigma_i(\bar{\mathcal{Z}}_\Phi) \sigma_i(\bar{\mathcal{Y}}_\Phi) - \Upsilon^\#(\mathcal{Y}) \right) \\ &= \sup_{\mathcal{Y}} \left(\sum_{i=1}^{n_{(2)}n_3} \sigma_i(\bar{\mathcal{Z}}_\Phi) \sigma_i(\bar{\mathcal{Y}}_\Phi) - \left(\sum_{i=1}^q \sigma_i(\bar{\mathcal{Y}}_\Phi) - q \right) \right) \\ &= \sup_{\mathcal{Y}} \left(\sigma_1(\bar{\mathcal{Y}}_\Phi) (\sigma_1(\bar{\mathcal{Z}}_\Phi) - 1) + \left(\sum_{i=2}^{n_{(2)}n_3} \sigma_i(\bar{\mathcal{Z}}_\Phi) \sigma_i(\bar{\mathcal{Y}}_\Phi) - \left(\sum_{i=2}^q \sigma_i(\bar{\mathcal{Y}}_\Phi) - q \right) \right) \right) \end{aligned}$$

tends to infinity. In the second case, $\|\bar{\mathcal{Z}}_\Phi\| \leq 1$, if $\|\bar{\mathcal{Y}}_\Phi\| \leq 1$, we obtain that $\Upsilon^\#(\mathcal{Y}) = 0$ and the supremum is achieved at $\sigma_i(\bar{\mathcal{Y}}_\Phi) = 1, i = 1, \dots, n_{(2)}n_3$, which yields

$$\Upsilon^\#(\mathcal{Z}) = \sum_{i=1}^{n_{(2)}n_3} \sigma_i(\bar{\mathcal{Z}}_\Phi) = \|\mathcal{Z}\|_{\text{TTNN}}.$$

If $\|\bar{\mathcal{Y}}_\Phi\| > 1$, we can prove $\Upsilon^\#(\mathcal{Z}) \leq \|\mathcal{Z}\|_{\text{TTNN}}$. In fact,

$$\begin{aligned} & \sum_{i=1}^{n_{(2)}n_3} \sigma_i(\bar{\mathcal{Z}}_\Phi) \sigma_i(\bar{\mathcal{Y}}_\Phi) - \sum_{i=1}^q (\sigma_i(\bar{\mathcal{Y}}_\Phi) - 1) \\ = & \sum_{i=1}^q \sigma_i(\bar{\mathcal{Z}}_\Phi) \sigma_i(\bar{\mathcal{Y}}_\Phi) + \sum_{i=q+1}^{n_{(2)}n_3} \sigma_i(\bar{\mathcal{Z}}_\Phi) \sigma_i(\bar{\mathcal{Y}}_\Phi) - \sum_{i=1}^q (\sigma_i(\bar{\mathcal{Y}}_\Phi) - 1) - \sum_{i=1}^{n_{(2)}n_3} \sigma_i(\bar{\mathcal{Z}}_\Phi) + \sum_{i=1}^{n_{(2)}n_3} \sigma_i(\bar{\mathcal{Z}}_\Phi) \\ = & \sum_{i=1}^q (\sigma_i(\bar{\mathcal{Z}}_\Phi) - 1) (\sigma_i(\bar{\mathcal{Y}}_\Phi) - 1) + \sum_{i=q+1}^{n_{(2)}n_3} \sigma_i(\bar{\mathcal{Z}}_\Phi) (\sigma_i(\bar{\mathcal{Y}}_\Phi) - 1) + \sum_{i=1}^{n_{(2)}n_3} \sigma_i(\bar{\mathcal{Z}}_\Phi) \\ \leq & \sum_{i=1}^{n_{(2)}n_3} \sigma_i(\bar{\mathcal{Z}}_\Phi), \end{aligned}$$

which can be derived from

$$\sum_{i=1}^q (\sigma_i(\bar{\mathcal{Z}}_\Phi) - 1) (\sigma_i(\bar{\mathcal{Y}}_\Phi) - 1) \leq 0 \quad \text{and} \quad \sum_{i=q+1}^{n_{(2)}n_3} \sigma_i(\bar{\mathcal{Z}}_\Phi) (\sigma_i(\bar{\mathcal{Y}}_\Phi) - 1) \leq 0.$$

In summary, we can get

$$\Upsilon^\#(\mathcal{Z}) = \sum_{i=1}^{n_{(2)}n_3} \sigma_i(\bar{\mathcal{Z}}_\Phi) = \|\mathcal{Z}\|_{\text{TTNN}}$$

over the set $\|\mathcal{Z}\| \leq 1$.

In addition, the convex envelope of $\text{rank}_{\text{sum}}(\mathcal{X})$ on $\{\mathcal{X} \in \mathbb{C}^{n_1 \times n_2 \times n_3} \mid \|\mathcal{X}\| \leq c\}$ can be changed into $\text{rank}_{\text{sum}}(\mathcal{Y})$ on $\{\mathcal{Y} \in \mathbb{C}^{n_1 \times n_2 \times n_3} \mid \|\mathcal{Y}\| \leq 1\}$ by setting $\mathcal{Y} = \frac{1}{c}\mathcal{X}$.

Appendix B. Proof of Theorem 2

In this section, we provide the detailed proof of Theorem 2. The idea is to employ convex analysis to derive conditions in which one can check whether the pair $(\mathcal{L}_0, \mathcal{E}_0)$ is the unique minizer to (3.7), and to show that such conditions are met with overwhelming probability in the conditions of Theorem 2. Before giving the detailed proof, we need to introduce the sampling schemes, some useful lemmas, as well as the subgradients of tensor l_1 norm and transformed tubal nuclear norm used in Theorem 2, respectively.

Sampling Schemes

The sampling strategy used in Theorem 2 is the uniform sampling without replacement. There are other widely used sampling models, e.g., Bernoulli sampling, adaptive sampling and random sampling with replacement. To facilitate our proof, we will consider the independent and identically distributed (*i.i.d.*) *Bernoulli-Rademacher model*. More precisely, we assume $\Omega = \{(i, j, k) \mid \delta_{ijk} = 1\}$, where

δ'_{ijk} s are i.i.d. Bernoulli variables taking value one with probability ρ and zero with probability $1 - \rho$. Such a Bernoulli sampling is denoted by $\Omega \sim \text{Ber}(\rho)$ for short. As a proxy for uniform sampling, the probability of failure under Bernoulli sampling with $\rho = \frac{m}{n_1 n_2 n_3}$ closely approximates the probability of failure under uniform sampling.

Let a subset $\Lambda \subset \Omega$ be the corrupted entries of \mathcal{L}_0 and $\Gamma \subset \Omega$ be locations where data are available and clean. In a standard Bernoulli model, we suppose that

$$\Omega \sim \text{Ber}(\rho), \quad \Lambda \sim \text{Ber}(\gamma\rho), \quad \Gamma \sim \text{Ber}((1 - \gamma)\rho),$$

and the signs of the nonzero entries of \mathcal{E}_0 are deterministic. It has been shown to be much easier to work with a stronger assumption that the signs of the nonzero entries of \mathcal{E}_0 are independent symmetric ± 1 random variables (i.e., Rademacher random variables). We introduce two independent random subsets of Ω

$$\Lambda' \sim \text{Ber}(2\gamma\rho), \quad \Gamma' \sim \text{Ber}((1 - 2\gamma)\rho),$$

and it is convenient to consider $\mathcal{E}_0 = \mathcal{P}_\Gamma(\mathcal{E})$ for some fixed tensor \mathcal{E} . Assume that a random sign tensor \mathcal{M} has i.i.d. entries such that for any index (i, j, k) , $\mathbb{P}(\mathcal{M}_{i,j,k} = 1) = \mathbb{P}(\mathcal{M}_{i,j,k} = -1) = \frac{1}{2}$. Then $|\mathcal{E}| \circ \mathcal{M}$ has components with symmetric random signs. By introducing a new noise tensor $\mathcal{E}'_0 = \mathcal{P}_{\Gamma'}(|\mathcal{E}| \circ \mathcal{M})$ and using the standard derandomization theory [4, Theorem 2.3]), we have the following results.

Lemma 2 *Suppose that \mathcal{L}_0 obeys the conditions of Theorem 2 and $\mathcal{E}_0, \mathcal{E}'_0$ are given as above. If the recovery of $(\mathcal{L}_0, \mathcal{E}'_0)$ is exact with high probability, it is also exact with at least the same probability for the model with input data $(\mathcal{L}_0, \mathcal{E}_0)$.*

According to Lemma 2, we can equivalently assume that the nonzero entries have symmetric random signs and

$$\Lambda \sim \text{Ber}(2\gamma\rho), \quad \Gamma \sim \text{Ber}((1 - 2\gamma)\rho), \quad (5.27)$$

for the locations of nonzero and zero entries of \mathcal{E}_0 , respectively.

Useful Lemmas

Suppose that \mathcal{L}_0 satisfies

$$\mathcal{L}_0 = \mathcal{U} \diamond_{\Phi} \mathcal{S} \diamond_{\Phi} \mathcal{V}^H, \quad (5.28)$$

where $\mathcal{U} \in \mathbb{C}^{n_1 \times r \times n_3}$, $\mathcal{V} \in \mathbb{C}^{n_2 \times r \times n_3}$ are unitary tensors, respectively, and $\mathcal{S} \in \mathbb{C}^{r \times r \times n_3}$ is a diagonal tensor. Denote the set T by

$$T = \{\mathcal{U} \diamond_{\Phi} \mathcal{Y}^H + \mathcal{W} \diamond_{\Phi} \mathcal{V}^H \mid \mathcal{Y} \in \mathbb{C}^{n_2 \times r \times n_3}, \mathcal{W} \in \mathbb{C}^{n_1 \times r \times n_3}\}. \quad (5.29)$$

For any $\mathcal{Z} \in \mathbb{C}^{n_1 \times n_2 \times n_3}$, the projections onto T and its complementary are given as follows [51, Proposition 7.1]:

$$\begin{aligned} P_T(\mathcal{Z}) &= \mathcal{U} \diamond_{\Phi} \mathcal{U}^H \diamond_{\Phi} \mathcal{Z} + \mathcal{Z} \diamond_{\Phi} \mathcal{V} \diamond_{\Phi} \mathcal{V}^H - \mathcal{U} \diamond_{\Phi} \mathcal{U}^H \diamond_{\Phi} \mathcal{Z} \diamond_{\Phi} \mathcal{V} \diamond_{\Phi} \mathcal{V}^H, \\ P_{T^\perp}(\mathcal{Z}) &= (\mathcal{I}_{\Phi} - \mathcal{U} \diamond_{\Phi} \mathcal{U}^H) \diamond_{\Phi} \mathcal{Z} \diamond_{\Phi} (\mathcal{I}_{\Phi} - \mathcal{V} \diamond_{\Phi} \mathcal{V}^H). \end{aligned}$$

From the definition of $P_T(\mathcal{A})$, and recall the inner product of two tensors, we can derive the following results.

Lemma 3 *Suppose that T is defined as (5.29), then $\langle P_T(\mathcal{A}), \mathcal{B} \rangle = \langle \mathcal{A}, P_T(\mathcal{B}) \rangle$.*

It follows from Lemma 3 that $\langle P_T(\mathcal{A}), P_{T^\perp}(\mathcal{B}) \rangle = 0$, where \mathcal{A} and \mathcal{B} are arbitrary tensors with proper sizes. Furthermore, based on the transformed tensor incoherence conditions given in (3.8)-(3.9), we can prove the following results which will be used many times in the sequel.

Lemma 4 *Let $\mathcal{A} \in \mathbb{C}^{n_1 \times n_2 \times n_3}$ be an arbitrary tensor, and T be given as (5.29). Suppose that the transformed tensor incoherence conditions (3.8)-(3.9) are satisfied and denote $\vec{e}_i \diamond_{\Phi} \dot{e}_k \diamond_{\Phi} \vec{e}_j^H = (\mathcal{E}_{\Phi})_{ijk}$, then*

$$\|P_T(\vec{e}_i \diamond_{\Phi} \dot{e}_k \diamond_{\Phi} \vec{e}_j^H)\|_F^2 = \|P_T(\mathcal{E}_{\Phi})_{ijk}\|_F^2 \leq \frac{2\mu_0 r}{n_{(2)}}.$$

For any given tensor, we have $\mathcal{Z} \in \mathbb{C}^{n_1 \times n_2 \times n_3}$,

$$\begin{aligned} \Phi[P_T(\mathcal{Z})] &= \sum_{i,j,k} \langle \Phi[P_T(\mathcal{Z})], \mathcal{E}_{ijk} \rangle \mathcal{E}_{ijk} \\ &= \sum_{i,j,k} \left\langle \Phi[P_T(\mathcal{Z})], \Phi[\vec{e}_i \diamond_{\Phi} \dot{e}_k \diamond_{\Phi} \vec{e}_j^H] \right\rangle \Phi[\vec{e}_i \diamond_{\Phi} \dot{e}_k \diamond_{\Phi} \vec{e}_j^H] \\ &= \sum_{i,j,k} \langle P_T(\mathcal{Z}), (\mathcal{E}_{\Phi})_{ijk} \rangle \Phi[(\mathcal{E}_{\Phi})_{ijk}], \end{aligned}$$

where the last equality follows from the definition of tensor inner product. By applying Φ^H operation to the tubes along the third dimension of $\Phi[P_T(\mathcal{Z})]$ and $\Phi[\vec{e}_i \diamond_{\Phi} \dot{e}_k \diamond_{\Phi} \vec{e}_j^H]$, respectively, we get that

$$P_T(\mathcal{Z}) = \sum_{i,j,k} \langle P_T(\mathcal{Z}), (\mathcal{E}_{\Phi})_{ijk} \rangle (\mathcal{E}_{\Phi})_{ijk} = \sum_{i,j,k} \langle \mathcal{Z}, P_T((\mathcal{E}_{\Phi})_{ijk}) \rangle (\mathcal{E}_{\Phi})_{ijk}. \quad (5.30)$$

Moreover, setting $\Omega \sim \text{Ber}(\rho)$, then we have

$$\rho^{-1} P_T P_{\Omega} P_T(\mathcal{Z}) \rho^{-1} \sum_{i,j,k} \delta_{ijk} \langle \mathcal{Z}, P_T((\mathcal{E}_{\Phi})_{ijk}) \rangle P_T((\mathcal{E}_{\Phi})_{ijk}), \quad (5.31)$$

which implies

$$\rho^{-1} \overline{P_T P_{\Omega} P_T(\mathcal{Z})} = \rho^{-1} \sum_{i,j,k} \delta_{ijk} \langle \mathcal{Z}, P_T((\mathcal{E}_{\Phi})_{ijk}) \rangle \overline{P_T((\mathcal{E}_{\Phi})_{ijk})}.$$

Based on the tensor decomposition forms given in (5.30)-(5.31), and applying the methods used in [21], we can get the following three lemmas.

Lemma 5 *Suppose that $\Omega \sim \text{Ber}(\rho)$, and T is defined in (5.29). Then with high probability,*

$$\|\rho^{-1} \mathcal{P}_T \mathcal{P}_{\Omega} \mathcal{P}_T - \mathcal{P}_T\|_{op} \leq \epsilon,$$

provided that $\rho \geq C_0 \frac{\mu r \log(n_{(1)} n_3)}{n_{(2)}} \epsilon^{-2}$ for some numerical constant $C_0 > 0$.

Lemma 6 *Suppose that $\mathcal{Z} \in \mathbb{C}^{n_1 \times n_2 \times n_3}$ is a fixed tensor and $\Omega \sim \text{Ber}(\rho)$. Then with high probability,*

$$\|(\rho^{-1} \mathcal{P}_T \mathcal{P}_{\Omega} \mathcal{P}_T - \mathcal{P}_T) \mathcal{Z}\|_{\infty} \leq \epsilon \|\mathcal{Z}\|_{\infty}, \quad (5.32)$$

provided that $\rho \geq C_0 \frac{\mu r \log(n_{(1)} n_3)}{n_{(2)}} \epsilon^{-2}$ for some numerical constant $C_0 > 0$.

Lemma 7 Suppose that $\mathcal{Z} \in \mathbb{C}^{n_1 \times n_2 \times n_3}$ is a fixed tensor and $\Omega \sim \text{Ber}(\rho)$. Then with high probability,

$$\|(\mathcal{I}_{\Phi} - \rho^{-1} \mathcal{P}_{\Omega})\mathcal{Z}\| \leq C'_0 \sqrt{\frac{n_{(1)}n_3 \log(n_{(1)}n_3)}{\rho}} \|\mathcal{Z}\|_{\infty}, \quad (5.33)$$

provided that $\rho \geq C_0 \frac{\log(n_{(1)}n_3)}{n_{(2)}n_3}$ for some numerical constants $C_0, C'_0 > 0$.

The following lemma is similar to [30, Lemma 4.5] which provides an upper bound for the spectral norm (which is based on any unitary transform instead of FFT) of the tensors consisting of Bernoulli sign variables. For simplicity, we omit its proof.

Lemma 8 For the $n_1 \times n_2 \times n_3$ Bernoulli sign tensor \mathcal{M} whose entries are distributed as

$$\mathcal{M}_{ijk} = \begin{cases} 1, & \text{with probability } \frac{\rho}{2}, \\ 0, & \text{with probability } 1 - \rho, \\ -1, & \text{with probability } \frac{\rho}{2}, \end{cases} \quad (5.34)$$

there exists a function $\varphi(\rho)$ satisfying $\lim_{\rho \rightarrow 0^+} \varphi(\rho) = 0$, such that the following statement holds with high probability:

$$\|\mathcal{M}\| \leq \varphi(\rho) \sqrt{n_{(1)}n_3}. \quad (5.35)$$

Subgradients of tensor l_1 norm and transformed tubal nuclear norm

In the optimization model (3.7), tensor l_1 norm and transformed tubal nuclear norm are used. One of the main technical tools in analyzing the tensor norms minimization is the characterization of the subgradients. Then we list the subdifferential of tensor l_1 norm and a subset of the subdifferential of transformed tubal nuclear norm, respectively.

Suppose that $\mathcal{A}, \mathcal{G} \in \mathbb{C}^{n_1 \times n_2 \times n_3}$, the subdifferential of any norm $\|\mathcal{A}\|$ can be given by

$$\partial\|\mathcal{A}\| = \left\{ \mathcal{G} : \|\mathcal{B}\| \geq \|\mathcal{A}\| + \text{Re}(\langle \mathcal{G}, \mathcal{B} - \mathcal{A} \rangle), \forall \mathcal{B} \in \mathbb{C}^{n_1 \times n_2 \times n_3} \right\}. \quad (5.36)$$

Here $\text{Re}(\cdot)$ denotes the real part of a complex number. Let $\tilde{\Omega}$ denotes the locations such that \mathcal{A}_{ijk} are nonzeros.

Lemma 9 Suppose that $\mathcal{A}, \mathcal{G} \in \mathbb{C}^{n_1 \times n_2 \times n_3}$, denote $\partial\|\mathcal{A}\|_1$ as the subdifferential of $\|\cdot\|_1$ at \mathcal{A} which is supported on $\tilde{\Omega}$, then

$$\partial\|\mathcal{A}\|_1 = \left\{ \mathcal{G} : \mathcal{G} = \text{dir}(\mathcal{A}) + \mathcal{F}, \mathcal{P}_{\tilde{\Omega}}(\mathcal{F}) = 0, \|\mathcal{F}\|_{\infty} \leq 1 \right\}, \quad (5.37)$$

where $\text{dir}(\mathcal{A})$ is defined as

$$\text{dir}(\mathcal{A}_{ijk}) = \begin{cases} \frac{\mathcal{A}_{ijk}}{|\mathcal{A}_{ijk}|}, & \mathcal{A}_{ijk} \neq 0, \\ 0, & \mathcal{A}_{ijk} = 0. \end{cases}$$

Proof. For any $x \in \mathbb{C}$, the subdifferential of $|\cdot|$ is given by

$$\partial|x| = \begin{cases} x/|x|, & \text{if } x \neq 0, \\ [-1, 1], & \text{if } x = 0. \end{cases}$$

Since the each entries of $\|\mathcal{A}\|_1$ is separable, we can obtain easily that

$$\partial\|\mathcal{A}\|_1 = \left\{ \mathcal{G} : \mathcal{G} = \text{dir}(\mathcal{A}) + \mathcal{F}, \mathcal{P}_{\tilde{\Omega}}(\mathcal{F}) = 0, \|\mathcal{F}\|_{\infty} \leq 1 \right\}.$$

This completes the proof. \square

Lemma 10 Suppose that $\mathcal{A} \in \mathbb{C}^{n_1 \times n_2 \times n_3}$ has the tensor singular value decomposition as (5.28). Denote $\partial\|\mathcal{A}\|_{\text{TTNN}}$ as the subdifferential of $\|\cdot\|_{\text{TTNN}}$ at \mathcal{A} , then

$$\partial\|\mathcal{A}\|_{\text{TTNN}} \supseteq \{\mathcal{G} \in \mathbb{C}^{n_1 \times n_2 \times n_3} : \mathcal{G} = \mathcal{U} \diamond_{\Phi} \mathcal{V}^H + \mathcal{F}\}, \quad (5.38)$$

where $\mathcal{U}^H \diamond_{\Phi} \mathcal{F} = \mathcal{F}^H \diamond_{\Phi} \mathcal{V} = \mathbf{0}$ and $\|\mathcal{F}\| \leq 1$.

Proof. If $\mathcal{A} = \mathbf{0}$, then the result is obvious. We now assume $\mathcal{A} \neq \mathbf{0}$, and \mathcal{Y} is given as (5.38). It follows that

$$\text{Re}(\langle \mathcal{A}, \mathcal{Y} \rangle) = \text{Re}(\langle \mathcal{A}, \mathcal{U} \diamond_{\Phi} \mathcal{V}^H + \mathcal{F} \rangle) = \text{Re}(\langle \mathcal{A}, \mathcal{U} \diamond_{\Phi} \mathcal{V}^H \rangle) + \text{Re}(\langle \mathcal{A}, \mathcal{F} \rangle) = \|\mathcal{A}\|_{\text{TTNN}}.$$

Moreover,

$$\|\mathcal{Y}\| = \|\mathcal{U} \diamond_{\Phi} \mathcal{V}^H + \mathcal{F}\| = \max\{\|\mathcal{U} \diamond_{\Phi} \mathcal{V}^H\| + \|\mathcal{F}\|\} = 1.$$

Then \mathcal{Y} satisfies (5.36) which is saying that \mathcal{Y} a subgradient of the tensor transform nuclear norm at \mathcal{A} . \square

The argument of the proof of Theorem 2 can be divided into two steps. The first step is to show a sufficient condition for the pair $(\mathcal{L}_0, \mathcal{E}_0)$ to be the unique optimal solution to problem (3.7). The second step is to prove that when required assumption in Theorem 2 are satisfied, the sufficient conditions derive by the first step is satisfied. Now we give a sufficient condition for the pair $(\mathcal{L}_0, \mathcal{E}_0)$ to be the unique optimal solution to problem (3.7). The conditions are stated in terms of a dual variable \mathcal{Y} , which is given in Theorem 4.

Theorem 4 Assume that there is a tensor $\mathcal{Y} \in \mathbb{C}^{n_1 \times n_2 \times n_3}$ obeying

$$\begin{cases} \|\mathcal{P}_T(\mathcal{Y} + \lambda \text{dir}(\mathcal{E}_0) - \mathcal{U} \diamond_{\Phi} \mathcal{V}^H)\|_F \leq \frac{\lambda}{n_1 n_2 n_3^2}, \\ \|\mathcal{P}_{T^\perp}(\mathcal{Y} + \lambda \text{dir}(\mathcal{E}_0))\| \leq \frac{1}{2}, \\ \|\mathcal{P}_\Gamma(\mathcal{Y})\|_\infty \leq \frac{\lambda}{2}, \\ \mathcal{P}_{\Gamma^\perp}(\mathcal{Y}) = \mathbf{0}, \end{cases} \quad (5.39)$$

where $\lambda = 1/\sqrt{\rho n(1)n_3}$, then $(\mathcal{L}_0, \mathcal{E}_0)$ is the unique optimal solution to (3.7) when n_1, n_2, n_3 are sufficient large.

Proof. Let $f(\mathcal{L}, \mathcal{E}) := \|\mathcal{L}\|_{\text{TTNN}} + \lambda\|\mathcal{E}\|_1$. Given a feasible perturbation $(\mathcal{L}_0 + \mathcal{Z}, \mathcal{E}_0 - \mathcal{P}_\Omega(\mathcal{Z}))$, we will show that the objective function value $f(\mathcal{L}_0 + \mathcal{Z}, \mathcal{E}_0 - \mathcal{P}_\Omega(\mathcal{Z}))$ is strictly larger than $f(\mathcal{L}_0, \mathcal{E}_0)$ unless $\mathcal{Z} = \mathbf{0}$. Denote the transformed tensor SVD of $\mathcal{P}_{T^\perp}(\mathcal{Z})$ by $\mathcal{P}_{T^\perp}(\mathcal{Z}) = \mathcal{U}_\perp \diamond_{\Phi} \mathcal{S}_\perp \diamond_{\Phi} \mathcal{V}_\perp^H$. Since $\bar{\mathcal{U}}^H \bar{\mathcal{U}}_\perp = \mathbf{0}$ and $\bar{\mathcal{V}}^H \bar{\mathcal{V}}_\perp = \mathbf{0}$, we have

$$\|\mathcal{U} \diamond_{\Phi} \mathcal{V}^H + \mathcal{U}_\perp \diamond_{\Phi} \mathcal{V}_\perp^H\| = \|\bar{\mathcal{U}} \bar{\mathcal{V}}^H + \bar{\mathcal{U}}_\perp \bar{\mathcal{V}}_\perp^H\| = 1.$$

It follows from Lemmas 9 and 10 that

$$\begin{aligned} \|\mathcal{L}_0 + \mathcal{Z}\|_{\text{TTNN}} &\geq \text{Re}(\langle \mathcal{U} \diamond_{\Phi} \mathcal{V}^H + \mathcal{U}_\perp \diamond_{\Phi} \mathcal{V}_\perp^H, \mathcal{L}_0 + \mathcal{Z} \rangle) \\ &= \text{Re}(\langle \mathcal{U} \diamond_{\Phi} \mathcal{V}^H, \mathcal{L}_0 \rangle) + \langle \mathcal{U}_\perp \diamond_{\Phi} \mathcal{V}_\perp^H, \mathcal{P}_{T^\perp}(\mathcal{Z}) \rangle + \langle \mathcal{U} \diamond_{\Phi} \mathcal{V}^H, \mathcal{Z} \rangle \\ &= \|\mathcal{L}_0\|_{\text{TTNN}} + \|\mathcal{P}_{T^\perp}(\mathcal{Z})\|_{\text{TTNN}} + \text{Re}(\langle \mathcal{U} \diamond_{\Phi} \mathcal{V}^H, \mathcal{Z} \rangle), \end{aligned}$$

and

$$\begin{aligned} \|\mathcal{E}_0 - \mathcal{P}_\Omega(\mathcal{Z})\|_1 &= \|\mathcal{P}_\Omega(\mathcal{E}_0 - \mathcal{Z})\|_1 = \|\mathcal{P}_\Gamma(\mathcal{E}_0 - \mathcal{Z})\|_1 + \|\mathcal{P}_\Lambda(\mathcal{E}_0 - \mathcal{Z})\|_1 \\ &= \|\mathcal{P}_\Gamma(\mathcal{Z})\|_1 + \|\mathcal{E}_0 - \mathcal{P}_\Lambda(\mathcal{Z})\|_1 \geq \|\mathcal{P}_\Gamma(\mathcal{Z})\|_1 + \|\mathcal{E}_0\|_1 - \text{Re}(\langle \text{dir}(\mathcal{E}_0), \mathcal{P}_\Lambda(\mathcal{Z}) \rangle) \\ &\geq \|\mathcal{P}_\Gamma(\mathcal{Z})\|_1 + \|\mathcal{E}_0\|_1 - \text{Re}(\langle \text{dir}(\mathcal{E}_0), \mathcal{Z} \rangle). \end{aligned}$$

Therefore, we obtain that

$$\begin{aligned}
& f(\mathcal{L}_0 + \mathcal{Z}, \mathcal{E}_0 - \mathcal{P}_\Omega(\mathcal{Z})) - f(\mathcal{L}_0, \mathcal{E}_0) \\
&= \|\mathcal{L}_0 + \mathcal{Z}\|_{\text{TTNN}} + \lambda \|\mathcal{E}_0 - \mathcal{P}_\Omega(\mathcal{Z})\|_1 - \|\mathcal{L}_0\|_{\text{TTNN}} - \lambda \|\mathcal{E}_0\|_1 \\
&\geq \|\mathcal{P}_{T^\perp}(\mathcal{Z})\|_{\text{TTNN}} + \lambda \|\mathcal{P}_\Gamma(\mathcal{Z})\|_1 - \text{Re}\langle \lambda \text{dir}(\mathcal{E}_0) - \mathcal{U} \diamond_{\Phi} \mathcal{V}^H, \mathcal{Z} \rangle \\
&\geq \|\mathcal{P}_{T^\perp}(\mathcal{Z})\|_{\text{TTNN}} + \lambda \|\mathcal{P}_\Gamma(\mathcal{Z})\|_1 - \text{Re}\langle \mathcal{P}_T(\mathcal{Y}), \mathcal{P}_\Gamma(\mathcal{Z}) \rangle \\
&\quad - \text{Re}\langle \mathcal{P}_T(\mathcal{Y} + \lambda \text{dir}(\mathcal{E}_0) - \mathcal{U} \diamond_{\Phi} \mathcal{V}^H), \mathcal{P}_T(\mathcal{Z}) \rangle - \text{Re}\langle \mathcal{P}_{T^\perp}(\mathcal{Y} + \lambda \text{dir}(\mathcal{E}_0)), \mathcal{P}_{T^\perp}(\mathcal{Z}) \rangle \\
&= \|\mathcal{P}_{T^\perp}(\mathcal{Z})\|_{\text{TTNN}} + \lambda \|\mathcal{P}_\Gamma(\mathcal{Z})\|_1 - \text{Re}\langle \mathcal{P}_\Gamma(\mathcal{Y}), \mathcal{P}_\Gamma(\mathcal{Z}) \rangle \\
&\quad - \text{Re}\langle \overline{\mathcal{P}_T(\mathcal{Y} + \lambda \text{dir}(\mathcal{E}_0) - \mathcal{U} \diamond_{\Phi} \mathcal{V}^H)}, \overline{\mathcal{P}_T(\mathcal{Z})} \rangle - \text{Re}\langle \overline{\mathcal{P}_{T^\perp}(\mathcal{Y} + \lambda \text{dir}(\mathcal{E}_0))}, \overline{\mathcal{P}_{T^\perp}(\mathcal{Z})} \rangle \\
&\geq \|\mathcal{P}_{T^\perp}(\mathcal{Z})\|_{\text{TTNN}} + \lambda \|\mathcal{P}_\Gamma(\mathcal{Z})\|_1 - \|\mathcal{P}_\Gamma(\mathcal{Y})\|_\infty \|\mathcal{P}_\Gamma(\mathcal{Z})\|_1 \\
&\quad - \|\overline{\mathcal{P}_T(\mathcal{Y} + \lambda \text{dir}(\mathcal{E}_0) - \mathcal{U} \diamond_{\Phi} \mathcal{V}^H)}\|_F \|\overline{\mathcal{P}_T(\mathcal{Z})}\|_F - \|\overline{\mathcal{P}_{T^\perp}(\mathcal{Y} + \lambda \text{dir}(\mathcal{E}_0))}\| \|\overline{\mathcal{P}_{T^\perp}(\mathcal{Z})}\|_* \\
&= \|\mathcal{P}_{T^\perp}(\mathcal{Z})\|_{\text{TTNN}} + \lambda \|\mathcal{P}_\Gamma(\mathcal{Z})\|_1 - \|\mathcal{P}_\Gamma(\mathcal{Y})\|_\infty \|\mathcal{P}_\Gamma(\mathcal{Z})\|_1 \\
&\quad - \|\mathcal{P}_T(\mathcal{Y} + \lambda \text{dir}(\mathcal{E}_0) - \mathcal{U} \diamond_{\Phi} \mathcal{V}^H)\|_F \|\mathcal{P}_T(\mathcal{Z})\|_F - \|\mathcal{P}_{T^\perp}(\mathcal{Y} + \lambda \text{dir}(\mathcal{E}_0))\| \|\mathcal{P}_{T^\perp}(\mathcal{Z})\|_{\text{TTNN}} \\
&\geq \frac{1}{2} \|\mathcal{P}_{T^\perp}(\mathcal{Z})\|_{\text{TTNN}} + \frac{\lambda}{2} \|\mathcal{P}_\Gamma(\mathcal{Z})\|_1 - \frac{\lambda}{n_1 n_2 n_3^2} \|\mathcal{P}_T(\mathcal{Z})\|_F, \tag{5.40}
\end{aligned}$$

where the inequality (5.40) is due to (5.39). It follows from Lemma 5 that

$$\left\| \frac{1}{(1-2\gamma)\rho} \mathcal{P}_T \mathcal{P}_\Gamma \mathcal{P}_T - \mathcal{P}_T \right\|_{\text{op}} \leq \frac{1}{2},$$

which implies $\left\| \frac{1}{\sqrt{(1-2\gamma)\rho}} \mathcal{P}_T \mathcal{P}_\Gamma \right\|_{\text{op}} \leq \sqrt{3/2}$. Therefore, we get

$$\begin{aligned}
& \|\mathcal{P}_T(\mathcal{Z})\|_F = \|\overline{\mathcal{P}_T(\mathcal{Z})}\|_F \\
&\leq 2 \left\| \frac{1}{(1-2\gamma)\rho} \overline{\mathcal{P}_T \mathcal{P}_\Gamma \mathcal{P}_T(\mathcal{Z})} \right\|_F \leq 2 \left\| \frac{1}{(1-2\gamma)\rho} \overline{\mathcal{P}_T \mathcal{P}_\Gamma \mathcal{P}_{T^\perp}(\mathcal{Z})} \right\|_F + 2 \left\| \frac{1}{(1-2\gamma)\rho} \overline{\mathcal{P}_T \mathcal{P}_\Gamma(\mathcal{Z})} \right\|_F \\
&\leq \sqrt{\frac{6}{(1-2\gamma)\rho}} \|\mathcal{P}_{T^\perp}(\mathcal{Z})\|_F + \sqrt{\frac{6}{(1-2\gamma)\rho}} \|\mathcal{P}_\Gamma(\mathcal{Z})\|_F. \tag{5.41}
\end{aligned}$$

It is easy to check that

$$\|\mathcal{P}_{T^\perp}(\mathcal{Z})\|_{\text{TTNN}} = \|\overline{\mathcal{P}_{T^\perp}(\mathcal{Z})}\|_* \geq \|\overline{\mathcal{P}_{T^\perp}(\mathcal{Z})}\|_F = \|\mathcal{P}_{T^\perp}(\mathcal{Z})\|_F \tag{5.42}$$

and $\|\mathcal{P}_\Gamma(\mathcal{Z})\|_1 \geq \|\mathcal{P}_\Gamma(\mathcal{Z})\|_F$. Substituting (5.41) and (5.42) into (5.40), we have

$$\begin{aligned}
& f(\mathcal{L}_0 + \mathcal{Z}, \mathcal{E}_0 - \mathcal{P}_\Omega(\mathcal{Z})) - f(\mathcal{L}_0, \mathcal{E}_0) \\
&\geq \left(\frac{1}{2} - \frac{\lambda}{n_1 n_2 n_3^2} \sqrt{\frac{6}{(1-2\gamma)\rho}} \right) \|\mathcal{P}_{T^\perp}(\mathcal{Z})\|_F + \left(\frac{\lambda}{2} - \frac{\lambda}{n_1 n_2 n_3^2} \sqrt{\frac{6}{(1-2\gamma)\rho}} \right) \|\mathcal{P}_\Gamma(\mathcal{Z})\|_F. \tag{5.43}
\end{aligned}$$

When n_1, n_2, n_3 are sufficiently large such that

$$\frac{1}{2} - \frac{\lambda}{n_1 n_2 n_3^2} \sqrt{\frac{6}{(1-2\gamma)\rho}} > 0, \quad \frac{\lambda}{2} - \frac{\lambda}{n_1 n_2 n_3^2} \sqrt{\frac{6}{(1-2\gamma)\rho}} > 0,$$

the inequality (5.43) holds if and only if $\mathcal{P}_{T^\perp}(\mathcal{Z}) = \mathcal{P}_\Gamma(\mathcal{Z}) = \mathbf{0}$. Thus, $\mathcal{P}_T \mathcal{P}_\Gamma(\mathcal{Z}) = \mathbf{0}$. On the other hand, when ρ is sufficiently large and γ is sufficiently small (which are bounded by two constants c_ρ and c_γ), we obtain that

$$\|\mathcal{P}_T \mathcal{P}_\Gamma\|_{\text{op}} \leq \sqrt{\frac{3(1-2\gamma)\rho}{2}} < 1,$$

which implies that $\mathcal{P}_T \mathcal{P}_\Gamma$ is injective. As a result, (5.43) holds if and only if $\mathcal{Z} = \mathbf{0}$. \square

Similar to [4] and [15], we use the golfing scheme to construct the dual tensor \mathcal{Y} , which is supported on Γ . Afterwards, the size of Γ is increased gradually. Consider the set $\Gamma \sim \text{Ber}((1 - 2\gamma)\rho)$ as a union of sets of support Γ_j , i.e.,

$$\Gamma = \bigcup_{j=1}^p \Gamma_j$$

where $\Gamma_j \sim \text{Ber}(q_j)$. Let $q_1 = q_2 = \frac{(1-2\gamma)\rho}{6}$ and $q_3 = \dots = q_p = q$, which implies $q \geq C_0\rho/\log(n_{(1)}n_3)$. Hence we have

$$1 - (1 - 2\gamma)\rho = \left(1 - \frac{(1 - 2\gamma)\rho}{6}\right)^2 (1 - q)^{p-2},$$

where $p = \lfloor 5 \log(n_{(1)}n_3) + 1 \rfloor$. Starting from $\mathcal{Z}_0 = \mathcal{P}_T(\mathcal{U} \diamond_{\Phi} \mathcal{V}^H - \lambda \text{sgn}(\mathcal{E}_0))$, we define inductively

$$\mathcal{Z}_j = \left(\mathcal{P}_T - \frac{1}{q_j} \mathcal{P}_T \mathcal{P}_{\Gamma_j} \mathcal{P}_T\right) \mathcal{Z}_{j-1}.$$

Then it follows from Lemmas 5-7 that

$$\|\mathcal{Z}_j\|_F \leq \frac{1}{2} \|\mathcal{Z}_{j-1}\|_F, \quad j = 1, \dots, p, \quad (5.44)$$

$$\|\mathcal{Z}_1\|_\infty \leq \frac{1}{2\sqrt{\log(n_{(1)}n_3)}} \|\mathcal{Z}_0\|_\infty, \quad (5.45)$$

$$\|\mathcal{Z}_j\|_\infty \leq \frac{1}{2^j \log(n_{(1)}n_3)} \|\mathcal{Z}_0\|_\infty, \quad j = 2, \dots, p, \quad (5.46)$$

and

$$\|(\mathcal{I}_{\Phi} - q_j^{-1} \mathcal{P}_{\Gamma_j}) \mathcal{Z}_{j-1}\| \leq C'_0 \sqrt{\frac{n_{(1)}n_3 \log(n_{(1)}n_3)}{q_j}} \|\mathcal{Z}_{j-1}\|_\infty, \quad j = 2, \dots, p, \quad (5.47)$$

with high probability provided c_r and c_γ are small enough.

Let the dual tensor \mathcal{Y} be

$$\mathcal{Y} = \sum_{j=1}^p \frac{1}{q_j} \mathcal{P}_{\Gamma_j}(\mathcal{Z}_{j-1}). \quad (5.48)$$

Then we need to show that the \mathcal{Y} in (5.48) satisfies (5.39). Obviously, $\mathcal{P}_{\Gamma^\perp}(\mathcal{Y}) = \mathbf{0}$ and it is sufficient to prove

$$\begin{cases} \|\mathcal{P}_T(\mathcal{Y} + \lambda \text{dir}(\mathcal{E}_0) - \mathcal{U} \diamond_{\Phi} \mathcal{V}^H)\|_F \leq \frac{\lambda}{n_1 n_2 n_3^2}, \\ \|\mathcal{P}_{T^\perp}(\mathcal{Y})\| \leq \frac{1}{4}, \\ \lambda \|\mathcal{P}_{T^\perp}(\text{dir}(\mathcal{E}_0))\| \leq \frac{1}{4}, \\ \|\mathcal{P}_\Gamma(\mathcal{Y})\|_\infty \leq \frac{\lambda}{2}, \end{cases} \quad (5.49)$$

where $\lambda = 1/\sqrt{\rho n_{(1)}n_3}$ and n_1, n_2, n_3 are large enough.

First, let us bound $\|\mathcal{Z}_0\|_F$ and $\|\mathcal{Z}_0\|_\infty$. By the triangle inequality, we get

$$\|\mathcal{Z}_0\|_\infty \leq \|\mathcal{U} \diamond_{\Phi} \mathcal{V}^H\|_\infty + \lambda \|\mathcal{P}_T(\text{dir}(\mathcal{E}_0))\|_\infty. \quad (5.50)$$

Note that $\mathcal{E}_{ijk} = \Phi[\vec{e}_i \diamond_{\Phi} \dot{e}_k \diamond_{\Phi} \vec{e}_j]$ and denote $(\mathcal{E}_{\Phi})_{ijk} = \vec{e}_i \diamond_{\Phi} \dot{e}_k \diamond_{\Phi} \vec{e}_j$, then

$$\text{dir}(\mathcal{E}_0) = \sum_{i,j,k} (\text{dir}(\mathcal{E}_0))_{i,j,k} \Phi[\vec{e}_i \diamond_{\Phi} \dot{e}_k \diamond_{\Phi} \vec{e}_j^H] = \sum_{i,j,k} (\text{dir}(\mathcal{E}_0))_{i,j,k} \Phi[(\mathcal{E}_{\Phi})_{ijk}].$$

Therefore, by (5.30) we have

$$\begin{aligned} \mathcal{P}_T(\text{dir}(\mathcal{E}_0)) &= \sum_{i,j,k} (\text{dir}(\mathcal{E}_0))_{i,j,k} \mathcal{P}_T(\Phi[\vec{e}_i \diamond_{\Phi} \dot{e}_k \diamond_{\Phi} \vec{e}_j^H]) \\ &= \sum_{i,j,k} (\text{dir}(\mathcal{E}_0))_{i,j,k} \langle \mathcal{E}_{ijk}, \mathcal{P}_T((\mathcal{E}_{\Phi})_{ijk}) \rangle (\mathcal{E}_{\Phi})_{ijk}. \end{aligned}$$

Hence, the (a, b, c) -th entry of $\mathcal{P}_T(\text{dir}(\mathcal{E}_0))$ can be represented by

$$\langle \mathcal{P}_T(\text{dir}(\mathcal{E}_0)), \Phi[\vec{e}_a \diamond_{\Phi} \dot{e}_b \diamond_{\Phi} \vec{e}_c^H] \rangle = \sum_{ijk} (\text{dir}(\mathcal{E}_0))_{i,j,k} \langle \mathcal{P}_T((\mathcal{E}_{\Phi})_{ijk}), \Phi[(\mathcal{E}_{\Phi})_{abc}] \rangle.$$

By Bernstein's inequality, we further have

$$\mathbb{P}(|\langle \mathcal{P}_T(\text{dir}(\mathcal{E}_0)), \Phi[(\mathcal{E}_{\Phi})_{ijk}] \rangle| \geq \tau) \leq 2 \exp\left(\frac{-\tau^2/2}{N + M\tau/3}\right),$$

where

$$M = \left| [\text{dir}(\mathcal{E}_0)]_{i,j,k} \right| \|\mathcal{P}_T((\mathcal{E}_{\Phi})_{ijk})\|_F \|\mathcal{P}_T((\mathcal{E}_{\Phi})_{abc})\|_F \leq \frac{2\mu r}{n_{(2)}},$$

and $N = 2\gamma\rho\|\mathcal{P}_T((\mathcal{E}_{\Phi})_{ijk})\|_F^2 \leq 4\gamma\rho\frac{\mu r}{n_{(2)}}$. Since the entries of $\mathcal{P}_T(\text{dir}(\mathcal{E}_0))$ can be understood as i.i.d. copies of the (a, b, c) -th entry, it follows from the union bound that

$$\|\mathcal{P}_T(\text{dir}(\mathcal{E}_0))\|_{\infty} \leq C'' \sqrt{\frac{\rho\mu r \log(n_{(1)}n_3)}{n_{(2)}}} \quad (5.51)$$

with high probability for some numerical constant C'' . By the joint incoherence condition (3.10), we obtain that

$$\|\mathcal{U} \diamond_{\Phi} \mathcal{V}^H\|_{\infty} \leq \sqrt{\frac{\mu r}{n_1 n_2 n_3}} = \lambda \sqrt{\frac{\rho\mu r}{n_{(2)}}}. \quad (5.52)$$

Therefore, combining (5.50), (5.51), and (5.52), we get

$$\|\mathcal{Z}_0\|_{\infty} \leq C\lambda \sqrt{\frac{\rho\mu r \log(n_{(1)}n_3)}{n_{(2)}}}, \quad (5.53)$$

$$\|\mathcal{Z}_0\|_F \leq \sqrt{n_1 n_2 n_3} \|\mathcal{Z}_0\|_{\infty} \leq C\lambda \sqrt{\rho\mu r n_{(1)} n_3 \log(n_{(1)}n_3)}, \quad (5.54)$$

where $C = \max\left\{\frac{1}{\log(n_{(1)}n_3)}, C''\right\}$.

Now, let us turn to the proof of (5.49). By (5.48), we obtain that

$$\begin{aligned}
& \|\mathcal{P}_T(\mathcal{Y}) + \mathcal{P}_T(\lambda \text{dir}(\mathcal{E}_0) - \mathcal{U} \diamond_{\Phi} \mathcal{V}^H)\|_F = \left\| \mathcal{Z}_0 - \sum_{j=1}^p \frac{1}{q_j} \mathcal{P}_T \mathcal{P}_{\Gamma_j}(\mathcal{Z}_{j-1}) \right\|_F \\
& = \left\| \left(\mathcal{P}_T - \frac{1}{q_1} \mathcal{P}_T \mathcal{P}_{\Gamma_1} \mathcal{P}_T \right) \mathcal{Z}_0 - \sum_{j=2}^p \frac{1}{q_j} \mathcal{P}_T \mathcal{P}_{\Gamma_j} \mathcal{P}_T(\mathcal{Z}_{j-1}) \right\|_F \\
& = \left\| \mathcal{P}_T(\mathcal{Z}_1) - \sum_{j=2}^p \frac{1}{q_j} \mathcal{P}_T \mathcal{P}_{\Gamma_j} \mathcal{P}_T(\mathcal{Z}_{j-1}) \right\|_F = \cdots = \|\mathcal{Z}_p\|_F \\
& \leq \left(\frac{1}{2} \right)^p \|\mathcal{Z}_0\|_F \leq C \left(n_{(1)} n_3 \right)^{-5} \lambda \sqrt{\rho \mu r n_{(1)} n_3 \log(n_{(1)} n_3)} \\
& \leq \frac{\lambda}{n_1 n_2 n_3^2},
\end{aligned}$$

where the first inequality follows from (5.44) and the second inequality from (5.54).

Furthermore, provided that $\lambda = 1/\sqrt{\rho n_{(1)} n_3}$ and c_r is sufficiently small, we have

$$\begin{aligned}
& \|\mathcal{P}_{T^\perp}(\mathcal{Y})\| = \left\| \mathcal{P}_{T^\perp} \sum_{j=1}^p \frac{1}{q_j} \mathcal{P}_{\Gamma_j}(\mathcal{Z}_{j-1}) \right\| \\
& \leq \sum_{j=1}^p \left\| \frac{1}{q_j} \mathcal{P}_{T^\perp} \mathcal{P}_{\Gamma_j}(\mathcal{Z}_{j-1}) \right\| = \sum_{j=1}^p \left\| \mathcal{P}_{T^\perp} \left(\frac{1}{q_j} \mathcal{P}_{\Gamma_j}(\mathcal{Z}_{j-1}) - \mathcal{Z}_{j-1} \right) \right\| \\
& \leq \sum_{j=1}^p \left\| \frac{1}{q_j} \mathcal{P}_{\Gamma_j}(\mathcal{Z}_{j-1}) - \mathcal{Z}_{j-1} \right\| \leq \sum_{j=1}^p C'_0 \sqrt{\frac{n_{(1)} n_3 \log(n_{(1)} n_3)}{q_j}} \|\mathcal{Z}_{j-1}\|_\infty \\
& \leq C'_0 \sqrt{n_{(1)} n_3 \log(n_{(1)} n_3)} \left(\sum_{j=3}^p \frac{1}{2^{j-1} \log(n_{(1)} n_3) \sqrt{q_j}} + \frac{1}{2 \sqrt{\log(n_{(1)} n_3) \sqrt{q_2}} + \frac{1}{\sqrt{q_1}}} \right) \|\mathcal{Z}_0\|_\infty \\
& \leq C' \lambda \sqrt{\frac{\rho \mu r n_{(1)} n_3 (\log(n_{(1)} n_3))^2}{\rho n_{(2)}}} \\
& \leq C' \sqrt{c_r} \leq \frac{1}{4},
\end{aligned}$$

where the third inequality follows from Lemma 7, the fourth inequality follows from (5.45)-(5.47), and the fifth inequality follows from (5.53), respectively.

Note that the direction tensor $\text{dir}(\mathcal{E}_0)$ satisfies

$$\left| [\text{dir}(\mathcal{E}_0)]_{i,j,k} \right| = \begin{cases} 1, & \text{with probability } \gamma \rho, \\ 0, & \text{with probability } 1 - \gamma \rho. \end{cases}$$

As proved by Lemma 8, there exists a function $\varphi(\gamma \rho)$ satisfying $\lim_{\gamma \rho \rightarrow 0^+} \varphi(\gamma \rho) = 0$, such that

$$\|\text{dir}(\mathcal{E}_0)\| \leq \varphi(\gamma \rho) \sqrt{n_{(1)} n_3}$$

with high probability, which yields

$$\lambda \|\mathcal{P}_{T^\perp}(\text{dir}(\mathcal{E}_0))\| \leq \lambda \|\text{dir}(\mathcal{E}_0)\| \leq \varphi(\gamma \rho) / \sqrt{\rho} \leq \frac{1}{4},$$

as long as c_r and c_γ is sufficiently small.

Finally, when c_r is small enough, we can get

$$\begin{aligned} \|\mathcal{P}_\Gamma(\mathcal{Y})\|_\infty &= \left\| \mathcal{P}_T \sum_{j=1}^p \frac{1}{q_j} \mathcal{P}_{\Gamma_j}(\mathcal{Z}_{j-1}) \right\|_\infty \leq \sum_{j=1}^p \frac{1}{q_j} \|\mathcal{Z}_{j-1}\|_\infty \\ &\leq \left(\sum_{j=3}^p \frac{1}{2^{j-1} \log(n_{(1)} n_3) \sqrt{q_j}} \right) \|\mathcal{Z}_0\|_\infty + \left(\frac{1}{2 \sqrt{\log(n_{(1)} n_3) q_2}} + \frac{1}{\sqrt{q_1}} \right) \|\mathcal{Z}_0\|_\infty \\ &\leq C \lambda \sqrt{\frac{\mu r \log(n_{(1)} n_3)}{\rho n_{(2)}}} \leq C \lambda \sqrt{\frac{c_r}{\log(n_{(1)} n_3)}} \leq \frac{\lambda}{2}, \end{aligned}$$

where the first inequality follows from Lemma 6, the second inequality follows from (5.45)-(5.47), and the third inequality follows from (5.53), respectively.

References

- [1] M. Bai, X. Zhang, G. Ni, and C. Cui. An adaptive correction approach for tensor completion. *SIAM J. Imaging Sci.*, 9(3):1298–1323, 2016.
- [2] J. A. Bengua, H. N. Phien, H. D. Tuan, and M. N. Do. Efficient tensor completion for color image and video recovery: Low-rank tensor train. *IEEE Trans. Image Process.*, 26(5):2466–2479, 2017.
- [3] J.-F. Cai, E. J. Candès, and Z. Shen. A singular value thresholding algorithm for matrix completion. *SIAM J. Optim.*, 20(4):1956–1982, 2010.
- [4] E. J. Candès, X. Li, Y. Ma, and J. Wright. Robust principal component analysis? *J. ACM*, 58(3):11, 2011.
- [5] E. J. Candès and B. Recht. Exact matrix completion via convex optimization. *Found. Comput. Math.*, 9(6):717–772, 2009.
- [6] L. Chen, D. Sun, and K.-C. Toh. An efficient inexact symmetric Gauss-Seidel based majorized ADMM for high-dimensional convex composite conic programming. *Math. Program.*, 161(1-2):237–270, 2017.
- [7] Y. Chen. Incoherence-optimal matrix completion. *IEEE Trans. Inf. Theory*, 61(5):2909–2923, 2015.
- [8] A. Cichocki, D. Mandic, L. De Lathauwer, G. Zhou, Q. Zhao, C. Caiafa, and H. A. Phan. Tensor decompositions for signal processing applications: From two-way to multiway component analysis. *IEEE Signal Process. Mag.*, 32(2):145–163, 2015.
- [9] L.-B. Cui, M.-H. Li, and Y. Song. Preconditioned tensor splitting iterations method for solving multi-linear systems. *Appl. Math. Letter*, 96:89–94, 2019.
- [10] I. Daubechies. *Ten Lectures on Wavelets*. PA, Philadelphia: SIAM, 1992.
- [11] H. Fan, J. Li, Q. Yuan, X. Liu, and M. K. Mg. Hyperspectral image denoising with bilinear low rank matrix factorization. *Signal Process.*, 163:132–152, 2019.
- [12] M. Fazel. *Matrix rank minimization with applications*. PhD thesis, PhD thesis, Stanford University, 2002.
- [13] S. Gandy, B. Recht, and I. Yamada. Tensor completion and low-n-rank tensor recovery via convex optimization. *Inverse Probl.*, 27(2):025010, 2011.
- [14] D. Goldfarb and Z. Qin. Robust low-rank tensor recovery: Models and algorithms. *SIAM J. Matrix Anal. Appl.*, 35(1):225–253, 2014.
- [15] D. Gross. Recovering low-rank matrices from few coefficients in any basis. *IEEE Trans. Inform. Theory*, 57(3):1548–1566, 2011.

- [16] Q. Gu, H. Gui, and J. Han. Robust tensor decomposition with gross corruption. In *Adv. Neural Inf. Process. Syst.*, pages 1422–1430, 2014.
- [17] W. Hu, D. Tao, W. Zhang, Y. Xie, and Y. Yang. The twist tensor nuclear norm for video completion. *IEEE Trans. Neural Netw. Learn. Syst.*, 28(12):2961–2973, 2017.
- [18] B. Huang, C. Mu, D. Goldfarb, and J. Wright. Provable models for robust low-rank tensor completion. *Pac. J. Optim.*, 11(2):339–364, 2015.
- [19] P. Jain and S. Oh. Provable tensor factorization with missing data. In *Adv. Neural Inf. Process. Syst.*, pages 1431–1439, 2014.
- [20] T.-Y. Ji, T.-Z. Huang, X.-L. Zhao, T.-H. Ma, and G. Liu. Tensor completion using total variation and low-rank matrix factorization. *Inf. Sci.*, 326:243–257, 2016.
- [21] J. Q. Jiang and M. K. Ng. Exact tensor completion from sparsely corrupted observations via convex optimization. *arXiv:1708.00601*, 2017.
- [22] L. Karlsson, D. Kressner, and A. Uschmajew. Parallel algorithms for tensor completion in the CP format. *Parallel Comput.*, 57:222–234, 2016.
- [23] E. Kernfeld, M. Kilmer, and S. Aeron. Tensor–tensor products with invertible linear transforms. *Linear Algebra Appl.*, 485:545–570, 2015.
- [24] M. E. Kilmer, K. Braman, N. Hao, and R. C. Hoover. Third-order tensors as operators on matrices: A theoretical and computational framework with applications in imaging. *SIAM J. Matrix Anal. Appl.*, 34(1):148–172, 2013.
- [25] M. E. Kilmer and C. D. Martin. Factorization strategies for third-order tensors. *Linear Algebra Appl.*, 435(3):641–658, 2011.
- [26] T. G. Kolda and B. W. Bader. Tensor decompositions and applications. *SIAM Rev.*, 51(3):455–500, 2009.
- [27] T. G. Kolda and J. Sun. Scalable tensor decompositions for multi-aspect data mining. In *Proc. 8th IEEE Int. Conf. Data Mining*, pages 363–372. IEEE, 2008.
- [28] X. Li, D. Sun, and K.-C. Toh. A Schur complement based semi-proximal admm for convex quadratic conic programming and extensions. *Math. Program.*, 155(1-2):333–373, 2016.
- [29] J. Liu, P. Musialski, P. Wonka, and J. Ye. Tensor completion for estimating missing values in visual data. *IEEE Trans. Pattern Anal. Mach. Intell.*, 35(1):208–220, 2013.
- [30] C. Lu, J. Feng, Y. Chen, W. Liu, Z. Lin, and S. Yan. Tensor robust principal component analysis: Exact recovery of corrupted low-rank tensors via convex optimization. In *Proc. IEEE Conf. Computer Vis. Pattern Recognit.*, pages 5249–5257, 2016.
- [31] C. Lu, J. Feng, Y. Chen, W. Liu, Z. Lin, and S. Yan. Tensor robust principal component analysis with a new tensor nuclear norm. *IEEE Trans. Pattern Anal. Mach. Intell.*, 2019.
- [32] C. D. Martin, R. Shafer, and B. LaRue. An order-p tensor factorization with applications in imaging. *SIAM J. Sci. Comput.*, 35(1):A474–A490, 2013.
- [33] F. Miwakeichi, P. A. Valdes-Sosa, E. Aubert-Vazquez, J. B. Bayard, J. Watanabe, H. Mizuhara, and Y. Yamaguchi. Decomposing EEG data into space-time-frequency components using parallel factor analysis and its relation with cerebral blood flow. In *Int. Conf. Neural Inf. Process.*, pages 802–810. Springer, 2007.
- [34] C. Mu, B. Huang, J. Wright, and D. Goldfarb. Square deal: Lower bounds and improved relaxations for tensor recovery. In *ICML*, volume 32, pages 73–81, 2014.
- [35] M. K. Ng, Q. Yuan, L. Yan, and J. Sun. An adaptive weighted tensor completion method for the recovery of remote sensing images with missing data. *IEEE Trans. Geosci. Remote Sens.*, 55(6):3367–3381, 2017.
- [36] T. D. Nguyen and G. Lee. Color image segmentation using tensor voting based color clustering. *Pattern Recognit. Lett.*, 33(5):605–614, 2012.

- [37] L. Omberg, G. H. Golub, and O. Alter. A tensor higher-order singular value decomposition for integrative analysis of DNA microarray data from different studies. *Proc. Natl. Acad. Sci. USA*, 104(47):18371–18376, 2007.
- [38] I. V. Oseledets. Tensor-train decomposition. *SIAM J. Sci. Comput.*, 33(5):2295–2317, 2011.
- [39] S. Oymak, A. Jalali, M. Fazel, Y. C. Eldar, and B. Hassibi. Simultaneously structured models with application to sparse and low-rank matrices. *IEEE Trans. Inform. Theory*, 61(5):2886–2908, 2015.
- [40] K. N. Plataniotis and A. N. Venetsanopoulos. *Color Image Processing and Applications*. Berlin: Springer, 2000.
- [41] S. Rabanser, O. Shchur, and S. Günnemann. Introduction to tensor decompositions and their applications in machine learning. *arXiv:1711.10781*, 2017.
- [42] B. Recht. A simpler approach to matrix completion. *J. Mach. Learn. Res.*, 12:3413–3430, 2009.
- [43] B. Recht, M. Fazel, and P. A. Parrilo. Guaranteed minimum-rank solutions of linear matrix equations via nuclear norm minimization. *SIAM Rev.*, 52(3):471–501, 2010.
- [44] B. Romera-Paredes and M. Pontil. A new convex relaxation for tensor completion. In *Adv. Neural Inf. Process. Syst.*, pages 2967–2975, 2013.
- [45] L. R. Tucker. Some mathematical notes on three-mode factor analysis. *Psychometrika*, 31(3):279–311, 1966.
- [46] B. Wang and H. Zou. Another look at distance-weighted discrimination. *J. Royal Stat. Soc. B*, 80(1):177–198, 2018.
- [47] Q. Xie, Q. Zhao, D. Meng, and Z. Xu. Kronecker-basis-representation based tensor sparsity and its applications to tensor recovery. *IEEE Trans. Pattern Anal. Mach. Intell.*, 40(8):1888–1902, 2018.
- [48] Y. Xu, R. Hao, W. Yin, and Z. Su. Parallel matrix factorization for low-rank tensor completion. *Inverse Probl. Imaging*, 9(2):601–624, 2013.
- [49] J.-H. Yang, X.-L. Zhao, T.-H. Ma, Y. Chen, T.-Z. Huang, and M. Ding. Remote sensing image destriping using unidirectional high-order total variation and nonconvex low-rank regularization. *J. Comput. Appl. Math.*, 363:124–144, 2020.
- [50] X. Zhang. A nonconvex relaxation approach to low-rank tensor completion. *IEEE Trans. Neural Netw. Learn. Syst.*, 30(6):1659–1671, 2019.
- [51] X. Zhang and M. K. Ng. A corrected tensor nuclear norm minimization method for noisy low-rank tensor completion. *SIAM J. Imaging Sci.*, 12(2):1231–1273, 2019.
- [52] Z. Zhang and S. Aeron. Exact tensor completion using t-SVD. *IEEE Trans. Signal Process.*, 65(6):1511–1526, 2017.
- [53] Z. Zhang, G. Ely, S. Aeron, N. Hao, and M. Kilmer. Novel methods for multilinear data completion and de-noising based on tensor-SVD. In *Proc. IEEE Conf. Computer Vis. Pattern Recognit.*, pages 3842–3849, 2014.
- [54] P. Zhou, C. Lu, Z. Lin, and C. Zhang. Tensor factorization for low-rank tensor completion. *IEEE Trans. Image Process.*, 27(3):1152–1163, 2018.
- [55] F. Zhu, Y. Wang, B. Fan, S. Xiang, G. Meng, and C. Pan. Spectral unmixing via data-guided sparsity. *IEEE Trans. Image Process.*, 23(12):5412–5427, 2014.